Matrix Diffusion as a Mechanism Contributing to Fractal Stream Chemistry

Harihar Rajaram[1,1]

[1]Johns Hopkins University

November 30, 2022

Abstract

Solute travel time distributions (TTDs) in catchments are relevant to both hydrochemical response and inference of hydrologic mechanisms. Time and frequency domain methods have been employed to estimate solute TTDs and associated power spectra. Stream concentration power spectra in some catchments exhibit fractal scaling (~1/frequency, or generally, 1/frequency to a power < 2). Various mechanisms have been proposed previously for fractal scaling. In several catchments, a significant fraction of streamflow is derived from groundwater in shallow fractured bedrock, where matrix diffusion significantly influences solute transport. I present frequency and time domain theoretical analyses of solute transport to quantify the influence of matrix diffusion on solute TTDs in catchment groundwater systems. The theoretical concentration power spectra exhibit fractal scaling, and the corresponding TTDs resemble a gamma distribution. An application to the Lower Hafren catchment using site-specific parameters shows that theoretical spectra match previously reported power spectral estimates derived from concentration measurements.

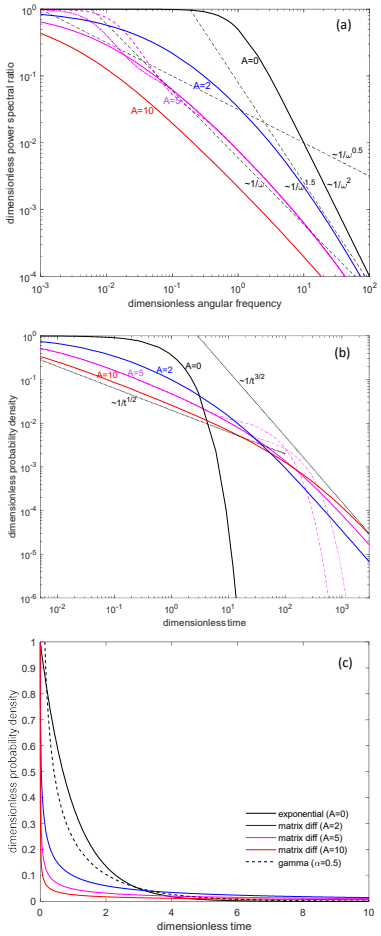

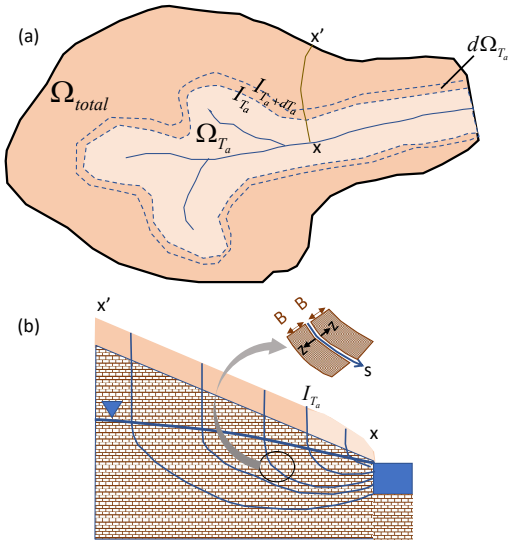

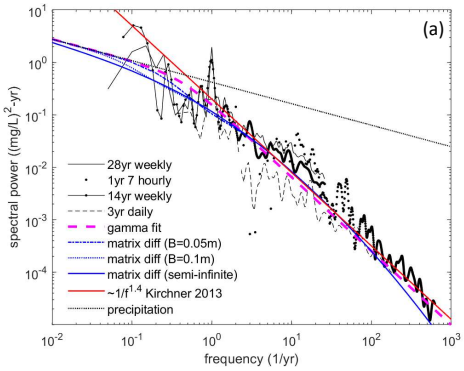

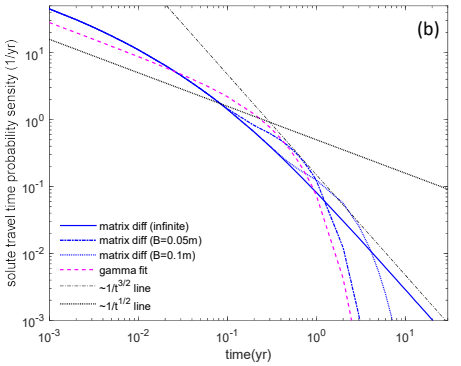

Matrix Diffusion as a Mechanism Contributing to Fractal Stream Chemistry

Harihar Rajaram[1]

[1]Department of Environmental Health and Engineering, Johns Hopkins University

Corresponding Author: Harihar Rajaram (hrajara1@jhu.edu)

Key Points:

- Influence of matrix diffusion on concentration power spectra and catchment solute travel time distributions is quantified theoretically
- Matrix diffusion is shown to produce fractal scaling in stream concentration power spectra when combined with variable advective travel times long streamlines
- 1/frequency spectral filtering identified in stream chloride power spectrum at Lower Hafren is reproduced by matrix diffusion model

Abstract

Solute travel time distributions (TTDs) in catchments are relevant to both hydrochemical response and inference of hydrologic mechanisms. Time and frequency domain methods have been employed to estimate solute TTDs and associated power spectra. Stream concentration power spectra in some catchments exhibit fractal scaling (~1/frequency, or generally, 1/frequency to a power < 2). Various mechanisms have been proposed previously for fractal scaling. In several catchments, a significant fraction of streamflow is derived from groundwater in shallow fractured bedrock, where matrix diffusion significantly influences solute transport. I present frequency and time domain theoretical analyses of solute transport to quantify the influence of matrix diffusion on solute TTDs in catchment groundwater systems. The theoretical concentration power spectra exhibit fractal scaling, and the corresponding TTDs resemble a gamma distribution. An application to the Lower Hafren catchment using site-specific parameters shows that theoretical spectra match previously reported power spectral estimates derived from concentration measurements.

Plain Language Summary

A significant fraction of rainfall on catchments flows as groundwater before discharging to a river. Groundwater in catchments is often hosted in shallow fractured bedrock. In these systems, solutes dissolved in rainfall are transported relatively rapidly by water flowing in rock fractures. However, some of the solute diffuses from fractures into the tiny pores of the rock matrix where water is stagnant. This phenomenon is referred to as matrix diffusion and leads to retention and slow long-term release of solutes. Solute transport and retention in catchments is relevant to understanding their response to contamination (e.g. by atmospheric deposition, agricultural chemicals) and inference of flow processes. This paper develops theoretical equations to

describe the transport and retention of solutes in catchments underlain by fractured bedrock, and the delivery of solutes to rivers. These theoretical equations explain interesting features of observed solute concentration variations in rivers and can be used to model catchment response to contamination.

1. Introduction

The transport and retention of solutes in catchments is influenced by both hydrologic and biogeochemical processes. Solute travel time distributions (TTDs) provide insights on integrated behavior of hydrologic and biogeochemical processes within catchments, although the distinction between the processes and time scales involved in hydrologic/hydraulic versus hydrochemical response should be emphasized (Maloszewski and Zuber, 1993; McGuire and McDonnell, 2006; Fiori and Russo, 2008; Botter et al. 2010; Birkel et al. 2011; Hrachowitz et al. 2013). There is a large body of research on TTDs in catchments, which has been synthesized in review papers (e.g. Maloszewski and Zuber, 1993; McGuire and McDonnell, 2006; Hrachowitz et al. 2016; Sprenger et al. 2019). Although TTDs were historically associated with steady flow systems, they have been generalized to unsteady flow using cumulative discharge transformation (Niemi, 1977; Rodhe et al. 1996), time variable travel/transit time distributions and storage selection functions (Sayama and McDonnell, 2009; Hrachowitz et al. 2010; Botter et al. 2011; van der velde et al. 2012; Harman, 2015).

One feature of catchment solute TTDs that has received much interest is that they often exhibit longer tails than the exponential distribution, a commonly used model for TTDs. Kirchner et al. (2000; 2001) analyzed the relationship between stream and precipitation concentration fluctuations of chloride in catchments at Plynlimon, U.K. They suggested that a gamma

60 distribution, $h(t) = \left(t^{\alpha-1}e^{-t/\beta}\right) / \left(\beta^{\alpha}\Gamma(\alpha)\right)$, with scale parameter $\alpha = 0.5$ (more generally $\alpha < 1$),
61 captures short-term responsiveness and long-tailed behavior and is hence a better model for
62 solute TTDs than the exponential distribution ($\alpha = 1$). Correspondingly, stream concentration
63 power spectra were observed to exhibit 1/frequency behavior (more generally 1/frequency to a
64 power < 2), which they referred to as "fractal stream chemistry". Similar behavior has been
65 documented at other catchments (Godsey et al. 2010), and for a variety of solutes (Kirchner et al.
66 2013), although some catchments do exhibit exponential baseflow TTDs (e.g. McGuire et al.
67 2005).

68 Various mechanisms have been proposed to explain fractal stream chemistry. Kirchner (2001)
69 showed that a model of advection-dispersion along a one-dimensional flowpath with distributed
70 solute inputs and a very large dispersivity (on the order of the hillslope length, equivalently
71 Peclet number (Pe) ~1), produces a solute TTD similar to a gamma distribution with $\alpha = 0.5$.
72 Lindgren et al. (2004) proposed that for moderate heterogeneity and dispersion, first-order
73 mobile-immobile exchange can explain fractal scaling. Both the above models assume uniform
74 mean flow and neglect nonuniform flow commonly associated with hillslope hydrologic systems.
75 Cardenas (2007) demonstrated that advection-dispersion in a nonuniform Tothian hillslope
76 groundwater flow (with significant variation in advective travel times across streamlines)
77 produces power-law solute TTDs. Kollett and Maxwell (2008) employed particle-tracking in
78 simulated flow fields for a real catchment to demonstrate that power-law stream concentration
79 spectra result even with very small dispersivities (Pe ~10^4), due to variations in advective travel
80 time across streamlines. They showed that transient vadose zone processes influence the stream
81 concentration spectra at higher frequencies. Fiori and Russo's (2008) simulations of transient
82 flow and solute transport in a hillslope produced TTDs resembling gamma distributions with $\alpha <$

1. Haitjema (1995) and Fiori and Russo (2008) showed that transient effects and heterogeneity have a minor influence on TTDs compared to variations in travel times across streamlines in steady flow representations. Ameli et al. (2016) showed that decreasing permeability with depth, either exponential or due to macroscopic layering, produced a gamma TTD with α close to 0.5. They also showed that in the absence of such heterogeneity, α is closer to 1. Harman (2015) showed that a time-variable uniform TTD with a range parameter that increases with decreasing storage (inverse storage effect) reproduces 1/frequency spectra. Lumped parameter hydrochemical models with multiple compartments have also reproduced gamma TTDs with $\alpha <$ 1 (Hrachowitz et al. 2013; Benettin et al. 2014).

The contribution of shallow groundwater flow through fractured bedrock to streamflow and solute export in mountain catchments has long been recognized, including at Plynlimon (Neal et al. 1997; Kirchner et al. 2001) and other recent studies (Godsey et al. 2010, Frisbee et al. 2013; Manning et al. 2014; Herndon et al. 2015; Hale et al. 2016; Tokunaga et al. 2019; Carroll et al. 2019; 2020). It is well established that matrix diffusion, a phenomenon first invoked to explain anomalous tracer ages (Foster, 1975; Neretnieks, 1981), significantly influences the travel time of tracers in fractured rock. The potential influence of matrix diffusion on catchment hydrochemical response and tracer ages was further highlighted by Maloszewski and Zuber (1993) and Shapiro (2011). However, few models of catchment-scale solute TTDs explicitly incorporate the influence of matrix diffusion. In this paper, I present frequency domain and time domain analyses of the combined influence of variable advective travel times and matrix diffusion on solute transport in a catchment/hillslope groundwater system hosted in fractured bedrock. I show that the theoretical power spectrum of stream concentration variations inherently exhibits fractal scaling, and that the solute TTD strongly resembles a gamma

106 distribution with $\alpha < 1$. I also present an application to the Lower Hafren catchment at
107 Plynlimon.

108 **2. Conceptual Model and Transport Equations**

109 The catchment-scale groundwater flow system is represented as a steady saturated flow in
110 fractured bedrock, receiving spatially uniform recharge. Figure 1 shows a schematic
111 representation (adapted from Haitjema, 1995). Fluid flow is assumed to occur only in fractures
112 with stagnant water in the rock matrix. Solutes undergo rapid advection along streamlines
113 through permeable fractures, while simultaneously diffusing in and out of the rock matrix. The
114 fracture density is assumed to be high so that an equivalent porous medium representation is
115 employed for flow (but not for transport). Thus, the water table and hydraulic head field are
116 assumed to be well defined and smooth. Isochrones I_{T_a} denote contours of equal advective
117 travel time T_a from the water table to the outflow at the stream, and Ω_{T_a} denotes the surface area
118 contained within I_{T_a}. Advective travel times T_a along streamlines (streamsurfaces) from the
119 water table to the stream are assumed to increase monotonically with Ω_{T_a}. The streamtube
120 originating from the surface element $d\Omega_{T_a}$ in Figure 1a is bounded by isochrones I_{T_a} and $I_{T_a+dT_a}$,
121 comprising streamlines along which advective travel times to the stream range from T_a to
122 $T_a + dT_a$. It is important to emphasize the distinction between advective and total solute travel
123 times: the total travel time along a streamline is also influenced by matrix diffusion and thus
124 much longer than the advective travel time. The catchment-scale solute TTD is derived by
125 considering the distribution of total travel times across all streamlines.

126 Previous studies suggest that when advective travel times across streamlines vary over a
127 large range, the influence of heterogeneity and dispersion is secondary (Gelhar, 1993; Duffy and
128 Gelhar, 1986; Haitjema, 1995; Fiori and Russo, 2008). I therefore neglect streamline tortuosity
129 and dispersion in the analysis presented below. Heterogeneity will lead to additional random
130 variations in advective travel times and may be incorporated using modified advective travel
131 time distributions as in the Lagrangian stochastic frameworks of Cvetkovic et al. (1999), Simic
132 and Destouni (1999) and Cvetkovic et al. (2012). I assume one-dimensional diffusion with an
133 effective matrix width *B* (Figure 1b), which may either be related to the block size or an
134 accessible weathered matrix thickness adjacent to fractures. Although matrix blocks in fractured
135 rock exhibit complex geometries, simplified solutions that assume one-dimensional matrix
136 diffusion (e.g. Tang et al. 1981; Maloszewski and Zuber, 1985) and various effective models
137 (Carrera et al. 1998; Cvetkovic et al. 1999; Haggerty et al. 2000; Berkowitz et al. 2006) are
138 widely used and have provided useful insights. Multi-dimensional diffusion in matrix blocks is
139 similar to one-dimensional diffusion with modified parameters, as discussed by Barker et al.
140 (1985).

141 For the above flow system, solute transport equations along a streamline and the stagnant
142 matrix domain adjacent to it are presented below, following Grisak and Pickens, (1980), Tang et
143 al. (1981), and Maloszweski and Zuber (1985). The fracture concentration at time t, at location s
144 along a streamline that originated at isochrone I_{T_a} (Figure 1) is denoted by $C_f(s,t;I_{T_a})$; and the
145 concentration in the adjacent rock matrix is denoted by $C_m(s,z,t;I_{T_a})$, where z is the distance
146 from the fracture matrix interface (see Figure 1b). The fracture transport equation is:

147 $$\frac{\partial C_f}{\partial t} + u_s \frac{\partial C_f}{\partial s} = \frac{2\phi_m D_e}{b} \frac{\partial C_m}{\partial z}\bigg|_{s,z=0,t} \qquad (1)$$

where u_s is the solute velocity along the streamline, b is the fracture aperture; ϕ_m and D_e are the matrix porosity and effective diffusivity respectively. The parameters b, ϕ_m and D_e are assumed as constant catchment-scale average values, while u_s varies across the flow system. The diffusion equation in the rock matrix is:

$$\left(\phi_m + \rho_b K_d\right)\frac{\partial C_m}{\partial t} - \phi_m D_e \frac{\partial^2 C_m}{\partial z^2} = 0 \qquad (2)$$

where ρ_b and K_d are respectively the bulk density of solids and the distribution coefficient in the rock matrix. The lateral boundary conditions for (2) are:

$$C_m(s, z=0, t; I_{T_a}) = C_f(s, t; I_{T_a}), \quad \frac{\partial C_m}{\partial z}(s, z=B, t; I_{T_a}) = 0 \qquad (3)$$

The streamline coordinate *s* in (1) may be replaced with an advective travel time coordinate (Gelhar and Collins, 1971; Duffy and Gelhar, 1986; Cvetkovic et al. 1999):

$$\tau_a = \int_{s'=0}^{s} \frac{ds'}{u_s(s')} \qquad (4)$$

Correspondingly, the fracture and matrix concentrations may be written as functions of τ_a, i.e. $C_f(\tau_a, t; I_{T_a})$ and $C_m(\tau_a, z, t; I_{T_a})$, and (1) can be rewritten as (Cvetkovic et al. 1999):

$$\frac{\partial C_f}{\partial t} + \frac{\partial C_f}{\partial \tau_a} = \frac{2\phi_m D_e}{b}\left.\frac{\partial C_m}{\partial z}\right|_{\tau_a, z=0, t} \qquad (5)$$

I use (5), together with (2) and (3) to relate the stream concentration to the input concentration. At the inflow end of a streamline (s = 0, τ_a = 0), concentration inputs $C_i(t)$ are assumed to be uniform across the catchment area (i.e. all streamlines), but vary with time:

$$C_f(\tau_a = 0, t; I_{T_a}) = C_i(t) \qquad (6)$$

At the outflow boundary, the stream concentration $C_o(t)$ is obtained by mixing of concentrations from all streamlines. The fraction of the total outflow that originates within the streamtube $d\Omega_{T_a}$ is denoted as $w(I_{T_a})d\Omega_{T_a}$, where $w(I_{T_a})$ is a flux-weighting function. If T_a increases monotonically with Ω_{T_a}, the fraction $w(I_{T_a})d\Omega_{T_a}$ may also be represented using the advective travel time probability density function across streamlines, $P(T_a)$, as $P(T_a)dT_a$. Thus $C_o(t)$ may be written in terms of an integral over either Ω_{T_a} or T_a:

$$C_o(t) = \int_{\Omega_{total}} C_f\left(T_a, t; I_{T_a}\right) w\left(I_{T_a}\right) d\Omega_{T_a} = \int_{T_a=0}^{\infty} C_f\left(T_a, t; I_{T_a}\right) P\left(T_a\right) dT_a \qquad (7)$$

If the fluid flux and velocity are assumed to be constant across the depth of the flow system at the outflow as in a Dupuit model, $w(I_{T_a}) = 1/\Omega_{total}$, a constant. Additionally assuming spatially uniform recharge and an approximately constant saturated thickness (H), $P(T_a)$ is an exponential distribution (Gelhar and Wilson, 1974; Maloszewski and Zuber, 1982; Haitjema, 1995):

$$P(T_a) = \frac{1}{\bar{T}_a} \exp\left(-\frac{T_a}{\bar{T}_a}\right) \qquad (8)$$

In (8), $\bar{T}_a$ is the mean advective travel time, given by $\phi_a H/r$, where ϕ_a is the active porosity corresponding to the hydrologically responsive fracture flow system and r is the recharge rate. The exponential advective travel time distribution is also applicable to hillslope flow systems with a sloping base, under the assumption of uniform recharge and constant saturated thickness. The relationship for Ω_{T_a} corresponding to (8) is (Haitjema, 1995):

183 $$\Omega_{T_a} = \Omega_{total}\left(1-\exp\left(-T_a/\overline{T}_a\right)\right) \qquad (9)$$

184 **3. Frequency Domain Analysis: Stream Concentration Power Spectrum**

185 To relate the power spectra of stream and precipitation concentrations, the transport equations
186 are solved in the frequency domain (SI, Sections S.1-2). The Fourier transforms of
187 $C_i(t), C_o(t), C_f(\tau_a, t; I_{T_a})$ and $C_m(\tau_a, z, t; I_{T_a})$ are denoted by $\tilde{C}_i(\omega), \tilde{C}_o(\omega), \tilde{C}_f(\tau_a, \omega; I_{T_a})$ and
188 $\tilde{C}_m(\tau_a, z, \omega; I_{T_a})$ respectively, where ω is the angular frequency. For random concentration
189 variations, the Fourier-Stieltjes spectral representation (Duffy and Gelhar, 1985, 1986; Gelhar,
190 1993), is more rigorous than the Fourier transform (Kirchner, 2000). However, both
191 interpretations involve the same mathematical manipulations and lead to identical concentration
192 power spectra. The Fourier transforms of (2-3) are solved to express $\tilde{C}_m(\tau_a, z, \omega; I_{T_a})$ in terms of
193 $\tilde{C}_f(\tau_a, \omega; I_{T_a})$ (S7 in SI). Using this relationship in the Fourier transform of (5) produces a
194 differential equation (S8 in SI) for $\tilde{C}_f(\tau_a, \omega; I_{T_a})$:

195 $$\frac{d\tilde{C}_f}{d\tau_a} + k(\omega)\tilde{C}_f = 0 \qquad (10)$$

196 where (S10-11 in SI):

197 $$k(\omega) = i\omega + \frac{2\phi_m\sqrt{RD_e\omega}}{b}\sqrt{i} - \frac{\frac{4\phi_m\sqrt{RD_e\omega}}{b}\sqrt{i}}{\left(1+\exp\left(2\sqrt{\frac{R\omega}{D_e}}B\sqrt{i}\right)\right)} \qquad (11)$$

198 In (11), $i = \sqrt{-1}$ and $R = (1+\rho_b K_d/\phi_m)$ denotes the retardation factor in the rock matrix.

Solving (10) and using the transform of (6), the Fourier transform of the fracture concentration at the outflow end of a streamline ($\tau_a = T_a$) is:

$$\tilde{C}_f(T_a, \omega; I_{T_a}) = \tilde{C}_i(\omega) \exp\{-k(\omega) T_a\} \qquad (12)$$

The Fourier transform of the stream concentration is then obtained from (7):

$$\tilde{C}_o(\omega) = \tilde{C}_i(\omega) \int_0^\infty \exp\{-k(\omega) T_a\} P(T_a) dT_a \qquad (13)$$

Correspondingly, the stream ($S_{C_o C_o}(\omega)$) and precipitation ($S_{C_i C_i}(\omega)$) concentration power spectra are related by:

$$S_{C_o C_o}(\omega) = S_{C_i C_i}(\omega) \left| \int_0^\infty \exp\{-k(\omega) T_a\} P(T_a)\, dT_a \right|^2 \qquad (14)$$

Equation (14) generalizes a relationship presented by Duffy and Gelhar (1985) and Gelhar (1993) for pure advection ($k(\omega) = i\omega$), by incorporating matrix diffusion and reformulating the integral in terms of $P(T_a)$. In general, any appropriate advective travel time distribution (obtained from an analytical or numerical groundwater flow model) can be employed in (14).

For the exponential advective travel time distribution, the stream concentration power spectrum is obtained by using (11) and (8) in (14) (Section S.2 in SI):

$$S_{C_o C_o}(\omega) = S_{C_i C_i}(\omega) \frac{1}{1 + 2\sqrt{2} AM \sqrt{\omega \overline{T_a}} + 2A^2 (M^2 + N^2) \omega \overline{T_a} + 2\sqrt{2} AN \left(\omega \overline{T_a}\right)^{3/2} + \omega^2 \overline{T_a}^2} \qquad (15)$$

where

$$A=\frac{\phi_m\sqrt{RD_e\overline{T_a}}}{b},\ m=1+\exp\left(\sqrt{2\omega\overline{T_a}}\,\frac{B\sqrt{R}}{\sqrt{D_e\overline{T_a}}}\right)\cos\left(\sqrt{2R\omega\overline{T_a}}\,\frac{B\sqrt{R}}{\sqrt{D_e\overline{T_a}}}\right)$$

$$n=\exp\left(\sqrt{2\omega\overline{T_a}}\,\frac{B\sqrt{R}}{\sqrt{D_e\overline{T_a}}}\right)\sin\left(\sqrt{2\omega\overline{T_a}}\,\frac{B\sqrt{R}}{\sqrt{D_e\overline{T_a}}}\right),\ M=1-\frac{2(m+n)}{m^2+n^2},\ N=1-\frac{2(m-n)}{m^2+n^2} \quad (16)$$

Equation (15) is written in terms of a dimensionless frequency ($\omega\overline{T_a}$) to highlight the dimensionless parameters that regulate the influence of matrix diffusion. The dimensionless parameter A is a measure of the strength of matrix diffusion. It may also be viewed as a ratio between a characteristic matrix storage over a time scale on the order of the mean advective travel time and the fracture storage. The parameter $B/\sqrt{D_e\overline{T}_a/R}$ represents the influence of matrix thickness. If B >> the characteristic matrix diffusion length ($\sqrt{D_e\overline{T}_a/R}$), the behavior is identical to that obtained with an infinite rock matrix thickness (M, $N\rightarrow 1$, Section S.2 in SI).

When the influence of matrix diffusion is strong (large A; M, N close to 1), the catchment spectral filter $S_{C_oC_o}/S_{C_iC_i}$ from (15) exhibits 1/frequency behavior (i.e. the third term in the denominator of (15) dominates). More generally, (15) can produce stream concentration power spectra with a range of apparent decay exponents > -2 (fractal scaling). When $A\rightarrow 0$ (negligible matrix diffusion) or $B\rightarrow 0$ (negligible matrix thickness), (15) reduces to $S_{C_oC_o}(\omega)=S_{C_iC_i}(\omega)/(1+\omega^2\overline{T_a}^2)$, which corresponds to pure advection with an exponential advective travel time distribution across streamlines (Gelhar, 1993). The well-mixed reservoir model also produces the same behavior (Gelhar and Wilson, 1974, Duffy and Gelhar, 1985, Gelhar, 1993, Kirchner et al. 2000).

232 Figure 2a shows the behavior of the spectral ratio $S_{C_oC_o} / S_{C_iC_i}$ for different values of A (0,

233 2, 5 and 10) and $B/\sqrt{De\overline{T}_a}$ (5, 10 and ∞) for $A = 5$, assuming no sorption $(R = 1)$. For context,

234 $A = 5$ would be obtained with $\phi_m = 0.05, D_e = 10^{-10}$ m^2/s, $b = 10^{-4}$ m, $\overline{T}_a = 12$ days, which are

235 realistic values. The mean total travel time is $\overline{T}_a\left(1 + 2B\phi_m / b\right) \approx$ 612 and 1212 days for

236 $B/\sqrt{De\overline{T}_a} = 5$ and 10, respectively. For an infinite matrix, the mean total travel time is

237 theoretically unbounded. For $A = 5$ and 10, the slope of the spectral ratio is close to -1 over

238 several orders of magnitude in frequency. For $A = 2$, the spectral ratio exhibits an apparent slope

239 close to -1 at intermediate dimensionless frequencies, approaching -1.5 at higher dimensionless

240 frequencies. In general, the spectral ratio in Figure 2a exhibits curvature and deviates from true

241 linear behavior in a log-log plot. However, the curvature is relatively mild at dimensionless

242 frequencies > 0.1. The scatter inherent in spectral estimates from noisy real-world data may

243 obscure such curvature and accommodate acceptable straight-line fits. A finite matrix width

244 does not influence the spectral ratio at high frequencies corresponding to time scales smaller than

245 the diffusion time scale across the width. At lower frequencies, spectral ratios for a finite matrix

246 width deviate from that for an infinite matrix and become steeper. This steepening could in fact

247 produce a closer tendency to straight-line behavior when estimating spectra from noisy data (see

248 *1/f* line plotted in Figure 2a).

249 A generalization of (15) for a gamma advective travel time distribution (e.g. representing

250 non-Dupuit flow) is presented in SI (S25, Section S.2). With a scale parameter α, the $1/\omega^{2\alpha}$

251 scaling in the spectral ratio of the advective travel time distribution is modified to $1/\omega^{\alpha}$ by

252 matrix diffusion. For a sorbing solute, (15) predicts that in the frequency range where the third

term in the denominator is dominant, the stream concentration power spectrum is *1/R* times that for a passive solute. This is consistent with the behavior suggested by Feng et al. (2004).

4. Time Domain Analysis: Solute Travel Time Distribution

The solute TTD $h(t)$ is the solution for $C_o(t)$ corresponding to a unit impulse (Dirac delta) input, i.e. $C_i(t) = \delta(t)$, and can be obtained from (7). The solution for $C_f(T_a, t; I_{T_a})$ at the outflow end of a streamline due to a unit impulse at the inflow, can be expressed in the form $H(t-T_a)g(T_a; t-T_a)$, where $H(t-T_a)$ is the Heaviside function. The function *g* depends on both the advective travel time T_a and the time since advective breakthrough, $t-T_a$. It has a simple analytical form for an infinite matrix (Maloszewski and Zuber, 1985; Section S.4 in SI):

$$g(T_a; t-T_a) = \frac{aT_a}{\sqrt{\pi}(t-T_a)^{3/2}} \exp\left(-\frac{a^2 T_a^2}{(t-T_a)}\right) \tag{17}$$

where $a = \phi_m \sqrt{RD_e}/b$. However, $g(T_a; t-T_a)$ can only be expressed as an implicit integral or obtained by numerical Laplace transform inversion for finite matrix widths (Maloszewski and Zuber, 1985; Section S.4 in SI). In either case, $h(t)$ can be expressed from (7) as:

$$h(t) = \int_0^\infty H(t-T_a)g(T_a; t-T_a)P(T_a)dT_a = \int_0^t g(T_a; t-T_a)P(T_a)dT_a \tag{18}$$

At any time *t* after input, the solute TTD (18) only includes contributions from streamlines for which the advective travel time to the stream $T_a \le t$. The solute TTD in (18) accounts for the combined influence of variable advective travel times across streamlines (with any appropriate form for $P(T_a)$) and matrix diffusion. Cvetkovic et al. (1999), Simic and Destouni (1999), Cvetkovic and Haggerty (2002), Lindgren et al. (2004) and Cvetkovic et al. (2012) employed

similar approaches to combine the influence of retention with advective travel time distributions generated by heterogeneity.

Figure 2b shows the dimensionless solute TTD $h\left(t/\overline{T}_a\right)\overline{T}_a$ obtained by numerical integration of (18) with the exponential $P(T_a)$ from (8). Analytical approximations can be derived for large times in the case of infinite matrix widths (SI Section S.4, for exponential and gamma $P(T_a)$). The TTD for $A = 0$ (no matrix diffusion) is the exponential distribution. For any value of A, at very early times $(t, T_a \to 0)$, $g\left(T_a; t-T_a\right) \to \delta\left(t-T_a\right)$ and $h(t) \to P(t)$, the advective travel time distribution. As A increases, solute breakthrough is attenuated to a greater extent by matrix diffusion. A power-law behavior $h(t) \sim t^{-1/2}$, similar to the gamma distribution with $\alpha = 0.5$, arises in an intermediate time regime for larger values of A (S35, SI Section S.4). For an infinite matrix, the late-time tail behaves as $h(t) \sim t^{-3/2}$ (SI Section S.4) and the mean total travel time is unbounded. For finite matrix widths (shown for A=5), the solute TTD coincides with that for an infinite width at times smaller than a characteristic diffusion time scale across the matrix width. It then levels off first, due to back-diffusion of solute from the matrix, and subsequently decreases exponentially as solute is flushed out, thus producing overall behavior resembling a gamma distribution with $\alpha = 0.5$. As noted above, the mean total travel time for finite matrix widths is $\overline{T}_a\left(1+2B\phi_m/b\right)$. Due to the explicit dependence of g on T_a, flowpaths with shorter T_a are less affected by matrix diffusion than flowpaths with longer T_a. As a result, $h(t)$ exhibits both short-term responsiveness and long-term memory, which are highlighted as salient properties of TTDs at Plynlimon (Krichner et al. 2000).

5. Application to the Lower Hafren Catchment

293 Neal et al. (1997) describe the hydrology and geology of the Hafren catchment. Storm
294 runoff is dominated by groundwater and interflow, and groundwater levels are highly responsive
295 to rainfall. The shallow groundwater system is hosted in highly fractured shale, mudstone, and
296 greywacke rocks, overlain by relatively thin soils (~0.7m). Typical water table depths are around
297 5m. Although groundwater is estimated to occur down to 30m below the stream, rapid
298 circulation and significant groundwater storage only occurs down to 9m depth, suggesting a
299 saturated thickness (H) of ~4m for the active portion of the groundwater system. The net
300 recharge rate (r) is about 2 m/year.

301 Kirchner (2000) and Kirchner et al. (2013) presented stream and precipitation power
302 spectra for chloride at Lower Hafren. The spectra presented by Kirchner et al. (2013) differ from
303 those of Kirchner (2000), due to refined spectral analysis methods and additional and longer
304 datasets. Both analyses suggest that the power spectral ratio $S_{C_oC_o}(\omega)/S_{C_iC_i}(\omega)$ exhibits close to
305 $1/\omega$ behavior. To represent this behavior, Kirchner et al. (2000) proposed a gamma distribution
306 for the solute TTD, for which $S_{C_oC_o}(f)/S_{C_iC_i}(f) = 1/(1+4\pi^2 f^2\beta^2)^{\alpha}$, where $f = \omega/2\pi$ is the
307 frequency. Kirchner et al. (2000) fitted values of $\alpha = 0.48,\ \beta = 1.9\,\mathrm{yr}$ to the observed power
308 spectra; which corresponds to a mean total travel time of $\alpha\beta = 0.91\,\mathrm{yr}$. The power spectra of
309 Kirchner et al. (2013) are better fit with $\alpha = 0.5,\ \beta = 0.4\,\mathrm{yr}$ (Figure 3a), which corresponds to a
310 shorter mean travel time of 0.2 years. Kirchner et al. (2013) reported that the precipitation
311 chloride spectrum exhibits $1/f^{0.41}$ behavior. From a precipitation spectrum based on a subset of
312 the full dataset (Harman, 2015), I obtained a best fit of $0.38/f^{0.34}$ (mg/L)^2-yr, and with the
313 exponent fixed at 0.41, I obtained a best fit $0.42/f^{0.41}$ (mg/L)^2-yr, which I used in the
314 calculations below. These two alternative forms for the precipitation chloride spectra do not

315 produce major differences in calculated stream concentration spectra (compare Figure 3a with
316 Figure S4 in SI).

317 The power spectral ratio (15, 16) depends on two key variables: the mean advective
318 travel time $\overline{T}_a$ and the matrix diffusion parameter A. Because A contains products and ratios of
319 other physical parameters, these parameters cannot be fit uniquely. My intention here is not to
320 produce a "best-fit" parameter set, but rather to present reasonable parameter values that are
321 consistent with the site description and match the spectral estimates of Kirchner et al. (2013). I
322 assume an exponential advective travel time distribution (8). Estimation of $\overline{T}_a$ requires an
323 estimate of the effective fracture porosity ϕ_a associated with the hydrologically responsive flow
324 system at the scale of the watershed, which is a highly uncertain parameter. Assuming a value of
325 $\phi_a = 0.005$, the mean advective travel time is estimated as $\overline{T}_a = \phi_a H / r = 0.01$ years (3.65 days).
326 To put this estimate in context, a regular arrangement of cubic matrix blocks with 0.3m sides,
327 interspersed with $b = 0.5mm$ wide connected fractures, would produce $\phi_a = 0.005$. The one-
328 dimensional accessible matrix width B in (15,16) could be smaller than the block size for two
329 reasons – first, Barker's (1985) analysis suggests an effective one-dimensional width equal to 1/6
330 of the block size for cubical blocks, and secondly, significant matrix diffusion is often restricted
331 to the weathered periphery of matrix blocks. Values for the matrix porosity ($\phi_m = 0.15$), and
332 effective diffusivity for chloride ($D_e = 1.5 \times 10^{-10}$ m^2/s), were assigned to fall within the ranges
333 reported for shale and mudstone (Manger, 1963; Barone et al. 1992). These parameter values
334 result in $A = 2.06$.

Figure 3a compares $S_{C_oC_o}(f)$ calculated using $S_{C_iC_i}(f) = 0.42 / f^{0.41}$ and the above parameter values in (15), the gamma model with $\alpha = 0.5$, $\beta = 0.4\,\mathrm{yr}$, and the power spectral estimates from Figure S7 in Kirchner et al. (2013). Both the matrix diffusion and the fitted gamma models produce reasonable matches to the estimated stream concentration spectra and the -1.4 slope estimated by Kirchner et al. (2013). Because of the relatively short $\bar{T}_a$, even an accessible matrix thickness as small as B = 0.05m ($B / \sqrt{De\bar{T}_a} = 7.27$) produces only a minor deviation of the power spectral ratio from that for the infinite matrix case. All models approach the precipitation concentration spectrum at frequencies < 0.1 yr^{-1}. At the high frequency end (> 20 yr^{-1}), the matrix diffusion models underestimate the spectral power slightly. This is likely because the analysis assumes steady flow and will thus miss the influence of hydrologic transients on solute transport. Alternative sets of parameter values that produce reasonable matches with the estimated stream concentration spectra are presented in SI (Figure S3). As noted above, compensatory variations among the physical parameters that occur in A preclude unique parameter estimates.

The solute TTDs corresponding to the power spectral models presented in Figure 3a are shown in Figure 3b. For finite matrix widths (B = 0.05 and 0.1m), the solute TTDs obtained with the matrix diffusion model are comparable to the fitted gamma distribution, which exhibits $t^{-1/2}$ power law behavior at intermediate times. The tails of the solute TTDs are longer for larger B, and for very large B, there is a tendency towards $t^{-3/2}$ behavior at late time. The mean solute travel times corresponding to the finite width matrix diffusion models are 0.31 years (B=0.05m) and 0.61 years (B=0.1m). Greater differences between the matrix diffusion models and the fitted

356 gamma model are evident in the TTD tails than in the low frequency behavior of the power
357 spectra.

358 **6. Discussion**

359 Although the role of matrix diffusion in influencing environmental solute ages has been
360 recognized previously, it is seldom explicitly considered in investigations and interpretations of
361 catchment solute TTDs. This paper quantitatively demonstrates that matrix diffusion in fractured
362 bedrock can generate fractal stream chemistry, and power-law behavior and long-term memory
363 in solute TTDs. The general relationships (14) and (18) provide a framework for quantifying
364 catchment-scale stream concentration power spectra and solute TTDs, by superposing the
365 influence of matrix diffusion on any general advective travel time distribution derived from
366 analytical or numerical subsurface flow models (e.g. Ameli et al. 2016; Kollett and Maxwell,
367 2008; Carroll et al. 2020). Availability of concentration data for multiple solutes will facilitate
368 inverse estimation of catchment-scale matrix diffusion parameters. The matrix diffusion
369 mechanism is physically consistent with the large residual or passive storage component inferred
370 while calibrating compartmental models of catchment hydrochemical response (e.g. Birkel et al.
371 2011, Benettin et al. 2014). The analysis presented here can be extended to incorporate
372 alternative representations of matrix diffusion and retention (e.g., multi-rate models or memory
373 functions) and heterogeneity within the fracture flow system (Cvetkovic and Haggerty, 2002;
374 Shapiro, 2001; Zhou et al. 2007), and layered hydrostratigraphy. One limitation of the analysis
375 is the neglect of transient flow effects and vadose zone processes, although some previous
376 studies (e.g. Fiori and Russo, 2008; Cvetkovic et al. 2012, Carroll et al. 2020) suggest that steady
377 state approximations are adequate for the dominant subsurface flow paths. Numerical models of
378 unsaturated-saturated flow and transport (e.g. Kollett and Maxwell, 2008; Carroll et al. 2020) can

be augmented to include matrix diffusion for more comprehensive evaluation of solute TTDs. Interpretation of solute TTDs, especially in mountain catchments with fractured bedrock, should consider the potential influence of matrix diffusion in addition to other factors.

Acknowledgements

This research was supported partially by National Science Foundation award EAR2012264. I am grateful to James Kirchner for providing the power spectral estimates from Lower Hafren, which are available in Figure S7 from Kirchner et al. (2013).

388 **References**

389 Ameli, A.A., Amvrosiadi, N., Grabs, T., Laudon, H., Creed, I.F. & McDonnell, J.J (2016).
390 Hillslope permeability architecture controls on subsurface transit time distribution and flow
391 paths. *Journal of Hydrology,* 543, 17-30. https://doi.org/10.1016/j.jhydrol.2016.04.071

392 Barone, F.S., Rowe, R.K., & Quigley, R.M. (1992). Estimation of chloride diffusion coefficient
393 and tortuosity factor for mudstone, *ASCE Journal of Geotechnical Engineering*, 118 (7), 1992,
394 https://doi.org/10.1061/(ASCE)0733-9410(1992)118:7(1031).

395 Barker, J.A. (1985). Block geometry functions characterizing transport in densely fissured
396 media. *Journal of Hydrology,* 77 (1985) 263-279. https://doi.org/10.1016/0022-1694(85)90211-2

397 Benettin, P., Kirchner, J.W., Rinaldo, A., & Botter, G. (2015) Modeling chloride transport using
398 travel time distributions at Plynlimon, Wales, *Water Resour. Res.*, 51, 3259–3276,
399 doi:10.1002/2014WR016600.

400 Berkowitz, B., Cortis, A., Dentz, M., & Scher, H. (2006). Modeling non-Fickian transport in
401 geological formations as a continuous time random walk. *Reviews of Geophysics*, *44*, RG2003.
402 https://doi.org/10.1029/2005rg000178

403 Birkel, C., Soulsby, C., & Tetzlaff, D. (2011). Modelling catchment-scale water storage
404 dynamics: Reconciling dynamic storage with tracer inferred passive storage, *Hydrol. Processes*,
405 25(25), 3924–3936, doi:10.1002/hyp.8201.

406 Botter, G., Bertuzzo, E., & Rinaldo, A. (2010). Transport in the hydrologic response: Travel time
407 distributions, soil moisture dynamics, and the old water paradox, *Water Resour. Res.*, 46,
408 W03514, doi:10.1029/2009WR008371.

Botter, G., Bertuzzo, E., & Rinaldo, A. (2011). Catchment residence and travel time distributions: The master equation, *Geophys. Res. Lett.*, 38, L11403, doi:10.1029/2011GL047666.

Cardenas, M. B. (2007). Potential contribution of topography-driven regional groundwater flow to fractal stream chemistry: Residence time distribution analysis of Toth flow, *Geophys. Res. Lett.*, 34, L05403, doi:10.1029/2006GL029126.

Carrera, J., Sanchez-Vila, X., Benet, I., Medina, A., Galarza, G., & Guimera, J. (1998). On matrix diffusion: Formulations, solution methods and qualitative effects. *Hydrogeology Journal*, *6*(1), 178–190. https://doi.org/10.1007/s100400050143

Carroll, R. W. H., Deems, J. S., Niswonger, R., Schumer, R., & Williams, K. H. (2019). The importance of interflow to groundwater recharge in a snowmelt-dominated headwater basin. *Geophysical Research Letters*, *46*, 5899–5908. https://doi.org/10.1029/2019GL082447

Carroll, R. W. H., Manning, A. H., Niswonger, R., Marchetti, D., & Williams, K. H. (2020). Baseflow age distributions and depth of active groundwater flow in a snow-dominated mountain headwater basin. *Water Resources Research*, *56*, e2020WR028161. https://doi.org/10.1029/2020WR028161

Cvetkovic, V., Selroos, J., & Cheng, H. (1999). Transport of reactive tracers in rock fractures. *J. Fluid Mech.*, 378 , 335-356, https://doi.org/10.1017/S0022112098003450

Cvetkovic, V., and R. Haggerty (2002), Transport with multiple-rate exchange in disordered media, Phys. Rev. E, 65, 051308, doi:10.1103/PhysRevE.65.051308.

Cvetkovic, V., Carstens, C., Selroos, J.-O., and Destouni, G. (2012). Water and solute transport along hydrological pathways, *Water Resour. Res.*, 48, W06537, doi:10.1029/2011WR011367.

Duffy, C. J., & Gelhar, L. W. (1985). A Frequency Domain Approach to Water Quality Modeling in Groundwater: Theory, *Water Resour. Res.*, 21(8), 1175– 1184, doi:10.1029/WR021i008p01175.

Duffy, C. J., & Gelhar, L. W. (1986). A Frequency Domain Analysis of Groundwater Quality Fluctuations: Interpretation of Field Data, *Water Resour. Res.*, 22(7), 1115– 1128, doi:10.1029/WR022i007p01115.

Feng, X., Kirchner, J.W., & Neal, C. (2004). Measuring catchment-scale chemical retardation using spectral analysis of reactive and passive chemical tracer time series, *Journal of Hydrology*, **292**, 296-307. https://doi.org/10.1016/j.jhydrol.2004.01.012.

Fiori, A., & Russo, D. (2008). Travel time distribution in a hillslope: Insight from numerical simulations, *Water Resour. Res.*, 44, W12426, doi:10.1029/2008WR007135.

Foster, S.S.D., (1975). The Chalk groundwater tritium anomaly — A possible explanation, *Journal of Hydrology*, 25 (1–2), 159-165, https://doi.org/10.1016/0022-1694(75)90045-1.

Frisbee, M. D., Wilson, J.L., Gomez-Velez, J.D., Phillips, F.M., & Campbell, A.R. (2013). Are we missing the tail (and the tale) of residence time distributions in watersheds?, *Geophys. Res. Lett.*, 40, 4633–4637, doi:10.1002/grl.50895.

Gelhar, L.W., (1993). *Stochastic Subsurface Hydrology*, Prentice-Hall, 390 pages. ISBN: 9780138467678

Gelhar, L. W., & Collins, M. A. (1971). General analysis of longitudinal dispersion in nonuniform flow. *Water Resources Research*, 7(6), 1511–1521. https://doi.org/10.1029/WR007i006p01511

Gelhar, L.W. and Wilson, J.L. (1974), Ground-Water Quality Modeling. *Groundwater*, 12: 399-408. https://doi.org/10.1111/j.1745-6584.1974.tb03050.x

Grisak, G., & Pickens, J.-F. (1980). Solute transport through fractured media: 1. The effect of matrix diffusion. *Water Resources Research*, *16*(4), 719-730. https://doi.org/10.1029/WR016i004p00719

Godsey, S.E., Aas, W., Clair, T.A., de Wit, H.A., Fernandez, I.J., Kahl, J.S., Malcolm, I.A., et al. (2010). Generality of fractal 1/f scaling in catchment tracer time series, and its implications for catchment travel time distributions. *Hydrol. Process.*, 24: 1660-1671. https://doi.org/10.1002/hyp.7677

Haggerty, R., McKenna, S. A., &Meigs, L. C. (2000). On the late-time behavior of tracer test breakthrough curves. *Water Resources Research*, *36*(12), 3467–3479. https://doi.org/10.1029/2000WR900214

Haitjema, H. M. (1995), On the residence time distribution in idealized groundwatersheds, *Journal of Hydrology*, 172(1– 4), 127– 146. https://doi.org/10.1016/0022-1694(95)02732-5

Hale, V. C., McDonnell, J. J., Stewart, M. K., Solomon, D. K., Doolitte, J., Ice, G. G., & Pack, R. T. (2016). Effect of bedrock permeability on stream base flow mean transit time scaling relationships: 2. Process study of storage and release, *Water Resour. Res.*, 52, 1375– 1397, doi:10.1002/2015WR017660.

Harman, C. J. (2015). Time-variable transit time distributions and transport: Theory and application to storage-dependent transport of chloride in a watershed, *Water Resour. Res.*, 51, 1–30, doi:10.1002/ 2014WR015707

Herndon, E. M., Dere, A. L.D., Sullivan, P. L., Norris, D., Reynolds, B., & Brantley, S. L. (2015). Landscape heterogeneity drives contrasting concentration–discharge relationships in shale headwater catchments, *Hydrol. Earth Syst. Sci.*, 19, 3333–3347, 2015 www.hydrol-earth-syst-sci.net/19/3333/2015/ doi:10.5194/hess-19-3333-2015.

Hrachowitz, M., Soulsby, C., Tetzlaff, D., Malcolm, I.A., & Schoups, G. (2010). Gamma distribution models for transit time estimation in catchments: Physical interpretation of parameters and implications for time-variant transit time assessment, *Water Resour. Res.*, 46, W10536, doi:10.1029/2010WR009148.

Hrachowitz, M., Savenije, H., Bogaard, T.A., Tetzlaff, D., & Soulsby, C. (2013). What can flux tracking teach us about water age distribution patterns and their temporal dynamics?, *Hydrol. Earth Syst. Sci.*, 17(2), 533–564, doi:10.5194/hess-17-533-2013.

Hrachowitz, M., Benettin, P., van Breukelen, B.M., Fovet, O., Howden, N.J., Ruiz, L., et al. (2016), Transit times—the link between hydrology and water quality at the catchment scale. *WIREs Water*, 3: 629-657. https://doi.org/10.1002/wat2.1155

Hyman, J. D., Rajaram, H., Srinivasan, S., Makedonska, N., Karra, S., Viswanathan, H., & Srinivasan, G. (2019). Matrix diffusion in fractured media: New insights into power law scaling of breakthrough curves. *Geophysical Research Letters*, 46, 13785– 13795. https://doi.org/10.1029/2019GL085454

491 Kirchner, J. W., Feng, X. H., & Neal, C. (2000). Fractal stream chemistry and its implications for
492 contaminant transport in catchments. *Nature*, 403(6769), 524–527.
493 https://doi.org/10.1038/35000537

494 Kirchner, J. W., Feng, X. H., & Neal, C. (2001). Catchment-scale advection and dispersion as a
495 mechanism for fractal scaling in stream tracer concentrations. *Journal of Hydrology*, 254(1-4),
496 82–101. https://doi.org/10.1016/S0022-1694(01)00487-5

497 Kirchner, J. W., & Neal, C. (2013). Universal fractal scaling in stream chemistry and its
498 implications for solute transport and water quality trend detection, *Proc. Natl. Acad. Sci. U. S. A.*,
499 110(30), 12,213–12,218, doi:10.1073/pnas.1304328110.

500 Kollet, S. J., & Maxwell, R.M. (2008). Demonstrating fractal scaling of baseflow residence time
501 distributions using a fully-coupled groundwater and land surface model, *Geophys. Res. Lett.*, 35,
502 L07402, doi:10.1029/2008GL033215.

503 Lindgren, G. A., Destouni, G., & Miller, A. V. (2004). Solute transport through the integrated
504 groundwater-stream system of a catchment, *Water Resour. Res.*, 40, W03511,
505 doi:10.1029/2003WR002765.

506 Manning, A. H., Verplanck, P. L., Caine, J. S. & Todd, A. S. (2013). Links between climate
507 change, water-table depth, and water chemistry in a mineralized mountain watershed. *Appl.*
508 *Geochem.* **37**, 64–78, https://doi.org/10.1016/j.apgeochem.2013.07.002.

509 Małoszewski, P., & Zuber, A. (1982). Determining the turnover time of groundwater systems
510 with the aid of environmental tracers: 1. Models and their applicability. Journal of Hydrology 57
511 (3–4) 207-231, https://doi.org/10.1016/0022-1694(82)90147-0

512 Małoszewski, P., & Zuber, A. (1985). On the theory of tracer experiments in fissured rocks with
513 a porous matrix. *Journal of Hydrology*, *79*(3-4), 333–358. https://doi.org/10.1016/0022-
514 1694(85)90064-2

515 Maloszewski, P., & Zuber, A. (1993). Principles and practice of calibration and validation of
516 mathematical models for the interpretation of environmental tracer data. *Advances in Water*
517 *Resources,* 16, 173–190. https://doi.org/10.1016/0309-1708(93)90036-F

518 Manger, G.E. (1963). Porosity and bulk density of sedimentary rocks, Geological Survey
519 Bulletin 1144-E, United States Geological Survey, https://pubs.usgs.gov/bul/1144e/report.pdf

520 McClure, T. (2020). Numerical Inverse Laplace Transform
521 (https://www.mathworks.com/matlabcentral/fileexchange/39035-numerical-inverse-laplace-
522 transform), MATLAB Central File Exchange. Retrieved October 4, 2020.

523 McGuire, K. J., McDonnell, J.J., Weiler, M., Kendall, C., McGlynn, B.L., Welker, J.M., &
524 Seibert, J. (2005). The role of topography on catchment-scale water residence time, *Water*
525 *Resour. Res.*, 41, W05002, doi:10.1029/2004WR003657.

526 McGuire, K.J., & McDonnell, J.J. (2006). A review and evaluation of catchment transit time
527 modeling, *Journal of Hydrology*, 330(3-4), 543–563. doi:10.1016/j.jhydrol.2006.04.020.

528 Neal, C., Robson, A. J., Shand, P., Edmunds, W. M., Dixon, A. J., Buckley, D. K., et. al. (1997).
529 The occurrence of groundwater in the Lower Palaeozoic rocks of upland Central Wales, *Hydrol.*
530 *Earth Syst. Sci.*, 1, 3–18, https://doi.org/10.5194/hess-1-3-1997.

531 Neretnieks, I. (1981), Age dating of groundwater in fissured rock: Influence of water volume in
532 micropores, *Water Resour. Res.*, 17(2), 421– 422, doi:10.1029/WR017i002p00421.

Neretnieks, I. (2006). Channeling with diffusion into stagnant water and into a matrix in series. *Water Resources Research*, *42*, W11418.

Niemi, A. J. (1977). Residence time distributions of variable flow processes, *Int. J. Appl. Radiat. Isotopes*, 28(10-11), 855–860, doi:10.1016/0020-708X(77)90026-6.

Rodhe, A., Nyberg, L., & Bishop, K. (1996). Transit times for water in a small till catchment from a step shift in the oxygen 18 content of the water input, *Water Resour. Res.*, 32(12), 3497–3511, doi:10.1029/95WR01806.

Sayama, T., & McDonnell, J. J. (2009). A new time-space accounting scheme to predict stream water residence time and hydrograph source components at the watershed scale, *Water Resour. Res.*, 45, W07401, doi:10.1029/2008WR007549.

Shapiro, A. M. (2001), Effective matrix diffusion in kilometer-scale transport in fractured crystalline rock, *Water Resour. Res.*, 37(3), 507– 522, doi:10.1029/2000WR900301.

Shapiro, A.M. The challenge of interpreting environmental tracer concentrations in fractured rock and carbonate aquifers. *Hydrogeol J* **19,** 9–12 (2011). https://doi.org/10.1007/s10040-010-0678-x

Simic, E., & Destouni, G. (1999). Water and solute residence times in a catchment: Stochastic-mechanistic model interpretation of 18O transport, *Water Resour. Res.*, 35(7), 2109– 2119, doi:10.1029/1999WR900054.

Sprenger, M., Stumpp, C., Weiler, M., Aeschbach, W., Allen, S. T., Benettin, P., et al. (2019). The demographics of water: A review of water ages in the critical zone. *Reviews of Geophysics*, 57, 800-834. https://doi.org/10.1029/ 2018RG000633

554 Tang, D., Frind, E., & Sudicky, E. A. (1981). Contaminant transport in fractured porous media:
555 Analytical solution for a single fracture. *Water Resources Research*, *17*(3), 555–564.
556 doi:10.1029/WR017i003p00555.

557 Tokunaga, T. K., Wan, J., Williams, K.H., Brown, W., Henderson, A., Kim, Y., et al. (2019).
558 Depth- and time-resolved distributions of snowmelt-driven hillslope subsurface flow and
559 transport and their contributions to surface waters. *Water Resources Research*, *55*,
560 https://doi.org/10.1029/2019WR025093

561 van der Velde, Y., Torfs, P.J.J.F., van der Zee, S.E.A.T.M, & Uijlenhoet, R. (2012). Quantifying
562 catchment-scale mixing and its effect on time-varying travel time distributions, *Water Resour.*
563 *Res.*, 48, W06536, doi:10.1029/2011WR011310.

564 Weisstein, Eric W. (2021) "Confluent Hypergeometric Function of the Second Kind."
565 From *MathWorld*-A Wolfram Web Resource.

566 https://mathworld.wolfram.com/ConfluentHypergeometricFunctionoftheSecondKind.html

567 Zhou, Q., Liu, H.-H., Molz, F. J., Zhang, Y., & Bodvarsson, G. S. (2007). Field-scale effective
568 matrix diffusion coefficient for fractured rock: Results from literature survey. *Journal of*
569 *Contaminant Hydrology*, *93*(1-4), 161–187. https://doi.org/10.1029/2005WR004448

570

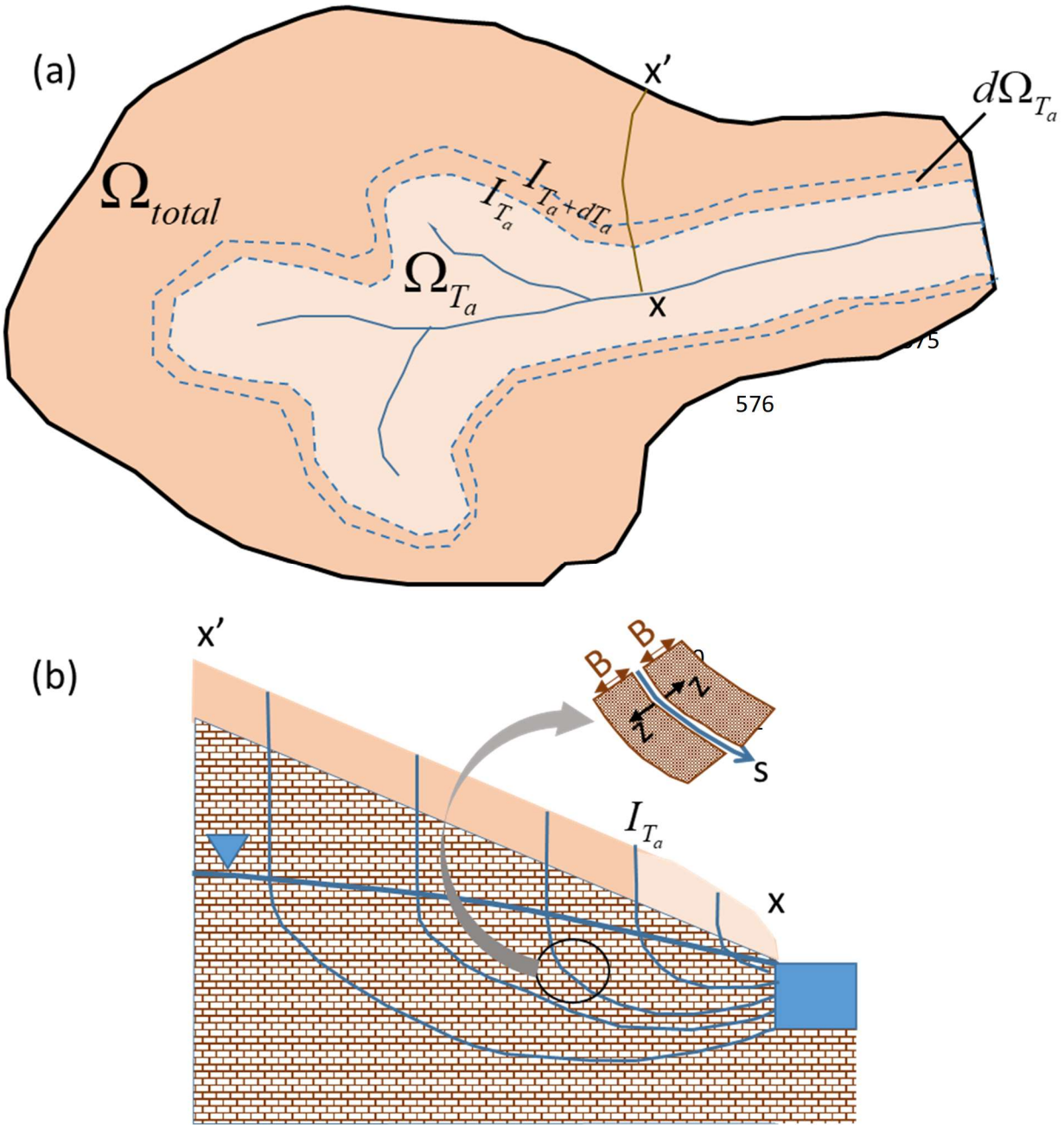

Figure 1. Schematic conceptual model of catchment-scale groundwater flow and transport. (a) Plan view showing total area Ω_{total} and area Ω_{T_a} bounded by isochrone I_{T_a} from which the advective travel time to the stream is T_a. (b) Vertical cross-section along x-x' in (a), showing streamlines from the surface, through the water table to the stream. The streamline coordinate is denoted by *s*, and *z* denotes the distance from the fracture-matrix interface. One-dimensional matrix diffusion is assumed, with an accessible matrix width *B*.

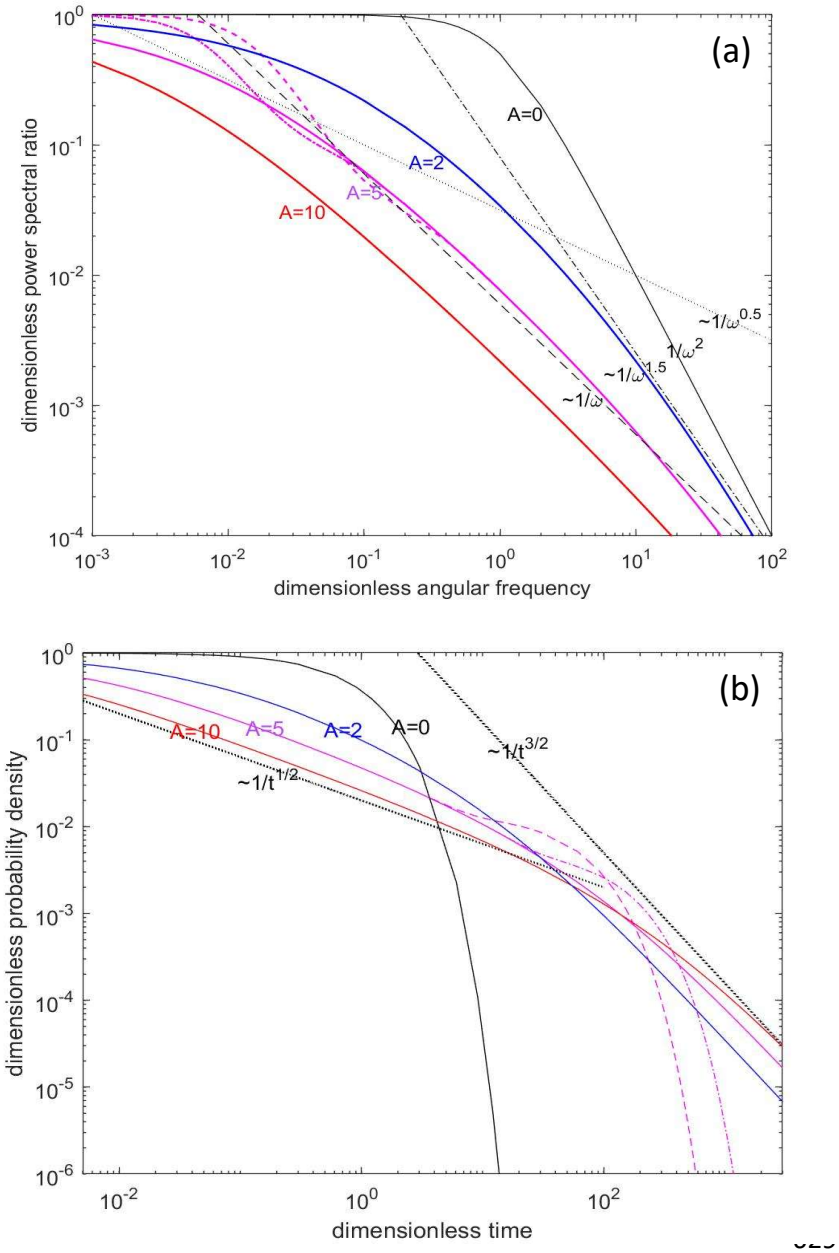

630

631 **Figure 2**. Influence of the matrix diffusion parameter A. (a) Dimensionless power spectral ratio
632 $\left(S_{C_oC_o} / S_{C_iC_i}\right)(15)$ plotted against dimensionless angular frequency ($\omega\overline{T_a}$). Black lines indicate
633 various power-law slopes. For $A=0$ (solid black), $S_{C_oC_o} / S_{C_iC_i}(\omega) = (1+\omega^2\overline{T_a}^2)$. (b)
634 Dimensionless solute TTD $h(t/\overline{T}_a)\overline{T}_a$ from (18) with an exponential $P(T_a)$, plotted against
635 dimensionless time ($t/\overline{T}_a$). Solid lines correspond to different values of A and an infinite matrix.
636 The dashed and dash-dotted magenta lines correspond to $B/\sqrt{D_e\overline{T}_a}$ = 5 and 10 respectively, for
637 A=5. Black dotted lines show intermediate ($\sim 1/t^{1/2}$) and late-time ($\sim 1/t^{3/2}$) power-law regimes.

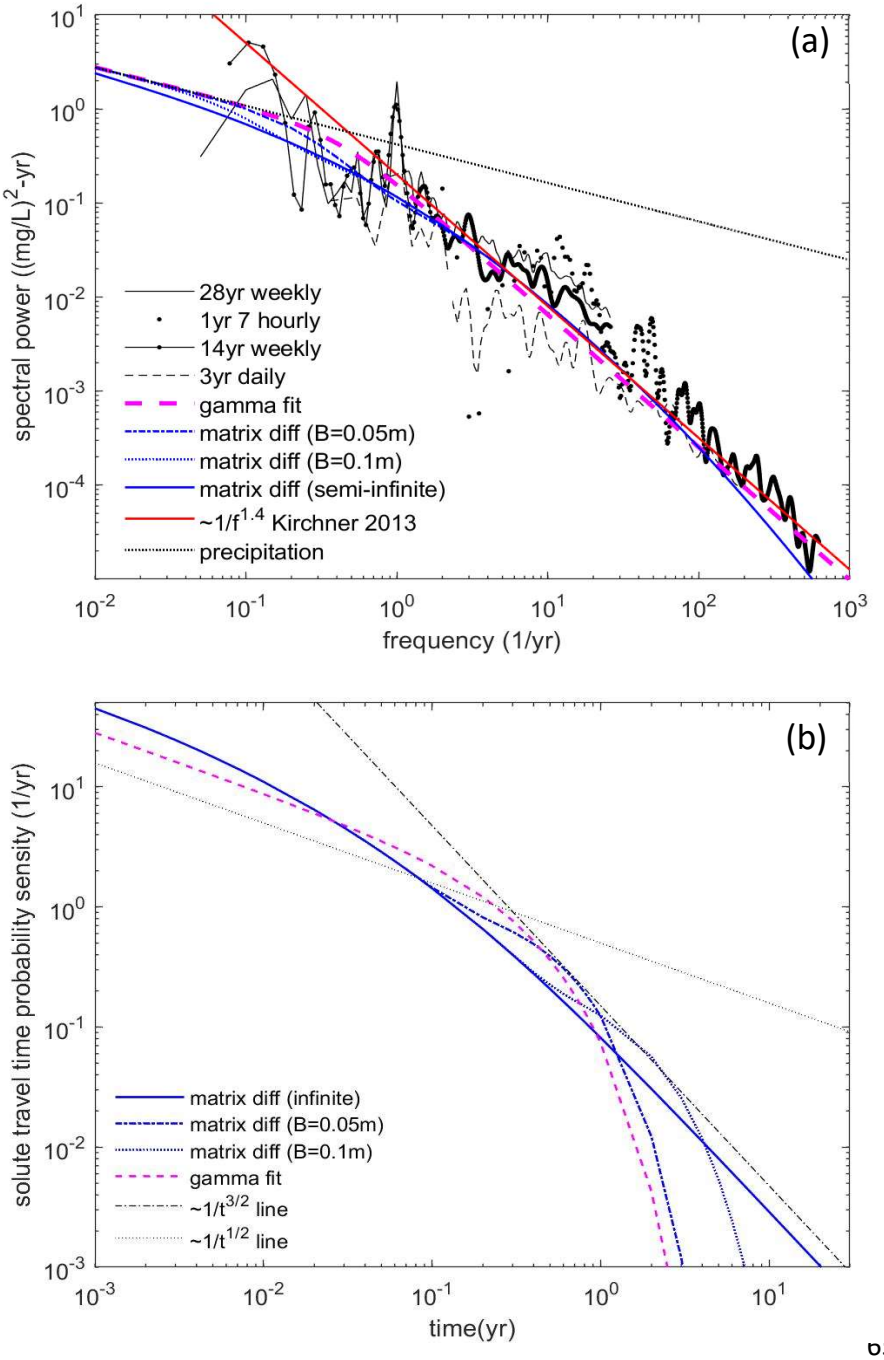

657

658 **Figure 3**. (a) Chloride power spectrum and (b) solute travel time distribution (TTD) for Lower
659 Hafren, based on the matrix diffusion model ($\phi_m = 0.15, D_e = 1.5\times10^{-10}\,\mathrm{m}^2/\mathrm{s}$, $b = 5\times10^{-4}\,\mathrm{m}$,
660 $\overline{T}_a = 0.01\mathrm{yr}$) and matrix widths $B = 0.05m, 0.1m$ and ∞; and a gamma model ($\alpha = 0.5, \beta = 0.4\mathrm{yr}$)
661 fit to the power spectral estimates from Kirchner et al. (2013). A line with the fitted power law
662 slope of -1.4 (Kirchner et al. 2013) is also shown in (a). Dotted and dash-dotted lines in (b)
663 respectively show the intermediate ($\sim 1/t^{1/2}$) and late-time ($\sim 1/t^{3/2}$) power-law regimes.

Geophysical Research Letters

Supporting Information for

Matrix Diffusion as a Mechanism Contributing to Fractal Stream Chemistry and Long-Tailed Transit Time Distributions

Harihar Rajaram[1]

[1]Department of Environmental Health and Engineering, Johns Hopkins University

Contents of this file

Introduction

Sections S.1 and S.2 provide detailed mathematical steps involved in the derivation of the key results pertaining to the stream concentration power spectrum (Equations (11-12) and (15)). Section S.2 includes a generalization of Equation (15) for the case of a gamma advective travel time distribution. Section S.3 provides a review of Laplace transforms (from previous literature), which are involved in the representation of the Green's function $g\left(T_a;t-T_a\right)$ needed for the evaluation of the solute TTD (Equation (18)) for finite matrix widths. Although the integral (Equation (18)) for the solute TTD can be evaluated exactly only by numerical integration, analytical approximations can be derived for infinite matrix width in three different dimensionless time regimes – these analytical approximations are presented in Section S.4, and provide additional insights into the power-law behavior of solute TTDs. Calculations of the stream concentration power spectrum for Lower Hafren, based on alternative parameter sets and an alternative precipitation concentration spectrum are presented in Section S.5.

S.1 Detailed Derivation of the Fourier Transform Solution for $\tilde{C}_f$ (Equations 11-12 in the manuscript)

The transport equation in the fracture is given by:

$$\frac{\partial C_f}{\partial t}+\frac{\partial C_f}{\partial \tau_a}=\frac{2\phi_m D_e}{b}\left.\frac{\partial C_m}{\partial z}\right|_{\tau_a, z=0, t} \qquad \text{(S1) (Equation 5 in the manuscript)}$$

The inflow boundary condition at the entrance to the streamline ($\tau_a = 0$) is:

$$C_f(\tau_a = 0, t; I_{T_a}) = C_i(t) \qquad \text{(S2) (Equation 6 in the manuscript)}$$

The right-hand side of (S1) may be evaluated by considering the diffusion equation in the rock matrix:

$$\left(\phi_m + \rho_b K_d\right)\frac{\partial C_m}{\partial t} - \phi_m D_e \frac{\partial^2 C_m}{\partial z^2} = 0 \qquad \text{(S3) (Equation 2 in the manuscript)}$$

Boundary conditions for (S3) are:

$$C_m(\tau_a, z = 0, t; I_{T_a}) = C_f(\tau_a, t; I_{T_a}), \quad \frac{\partial C_m}{\partial z}(\tau_a, z = B, t; I_{T_a}) = 0 \text{ (S4) (Equation 3 in the manuscript,}$$

with τ_a in place of *s*)

The notation $\tilde{C}_i(\omega), \tilde{C}_o(\omega), \tilde{C}_f(\tau_a, \omega; I_{T_a})$ and $\tilde{C}_m(\tau_a, z, \omega; I_{T_a})$ is used for the Fourier transforms of $C_i(t), C_o(t), C_f(\tau_a, t; I_{T_a})$ and $C_m(\tau_a, z, t; I_{T_a})$ respectively, with ω denoting the angular frequency.

The first step is to take the Fourier Transform of the matrix diffusion equation (S3) and boundary conditions (S4), which yields (S5) and (S6):

$$i\omega\tilde{C}_m - \frac{D_e}{R}\frac{d^2\tilde{C}_m}{dz^2} = 0 \qquad \text{(S5)}$$

where $R = (1 + \rho_b K_d / \phi_m)$ is the retardation factor in the matrix and $i = \sqrt{-1}$.

$$\tilde{C}_m(\tau_a, z=0, \omega; I_{T_a}) = \tilde{C}_f(\tau_a, \omega; I_{T_a}), \quad \frac{d\tilde{C}_m}{dz}(\tau_a, z=B, \omega; I_{T_a}) = 0 \quad \text{(S6)}$$

Equations (S5-S6) are then readily solved to obtain $\tilde{C}_m$ in terms of $\tilde{C}_f$:

$$\tilde{C}_m = \tilde{C}_f \left(\frac{e^{-\sqrt{i}uz} + e^{\sqrt{i}u(z-2B)}}{1 + e^{-2\sqrt{i}uB}} \right), \text{ where } u = \sqrt{\frac{\omega R}{D_e}} \quad \text{(S7)}$$

The Fourier transform of (S1) is:

$$i\omega\tilde{C}_f + \frac{d\tilde{C}_f}{d\tau_a} = \frac{2\phi_m D_e}{b} \left. \frac{\partial \tilde{C}_m}{\partial z} \right|_{\tau_a, z=0, \omega} \quad \text{(S8)}$$

The right hand side of (S8) involves the derivative of $\tilde{C}_m$ at the fracture-matrix interface ($z = 0$),

which can be obtained from (S7):

$$\left. \frac{\partial \tilde{C}_m}{\partial z} \right|_{\tau_a, z=0, \omega} = \tilde{C}_f(\tau_a, \omega) \left(-\sqrt{i}u + \frac{2\sqrt{i}u}{1 + e^{2\sqrt{i}uB}} \right) \quad \text{(S9)}$$

Using (S9) in (S8) yields the following first-order ordinary differential equation for $\tilde{C}_f$:

$$i\omega\tilde{C}_f + \frac{d\tilde{C}_f}{d\tau_a} = \frac{2\phi_m D_e}{b} \tilde{C}_f \left(-\sqrt{i}u + \frac{2\sqrt{i}u}{1 + e^{2\sqrt{i}uB}} \right) \quad \text{(S10)}$$

Equation (S10) can be rewritten as:

$$\frac{d\tilde{C}_f}{d\tau_a} + \left(i\omega + \frac{2\phi_m \sqrt{RD_e\omega}}{b}\sqrt{i} - \frac{\frac{4\phi_m \sqrt{RD_e\omega}}{b}\sqrt{i}}{\left(1 + \exp\left(2\sqrt{\frac{R\omega}{D_e}}B\sqrt{i}\right)\right)} \right) \tilde{C}_f = 0 \quad \text{(S11)}$$

With $k(\omega) = i\omega + \frac{2\phi_m \sqrt{RD_e\omega}}{b}\sqrt{i} - \frac{\frac{4\phi_m \sqrt{RD_e\omega}}{b}\sqrt{i}}{\left(1 + \exp\left(2\sqrt{\frac{R\omega}{D_e}}B\sqrt{i}\right)\right)}$, (Equation 11 in the manuscript)

the solution for $\tilde{C}_f$ is obtained in compact form as:

$$\tilde{C}_f(T_a,\omega;I_{T_a}) = \tilde{C}_i(\omega)\exp\{-k(\omega)T_a\} \quad \text{(S12) (Equation 12 in manuscript)}$$

S.2 Detailed Derivation of the Power Spectrum of Stream Concentration Variations $S_{C_oC_o}$ or catchment spectral filter $S_{C_oC_o}/S_{C_iC_i}$ (Equation 15 in the manuscript)

The Fourier transform of the stream (outflow) concentration, $\tilde{C}_o(\omega)$, can be obtained starting from Equations (13) and (8) in the manuscript:

$$\tilde{C}_o(\omega) = \tilde{C}_i(\omega)\int_0^\infty \exp\{-k(\omega)T_a\}P(T_a)dT_a \quad \text{(S13) (Equation 13 in manuscript)}$$

$$P(T_a) = \frac{1}{\overline{T}_a}\exp\left(-\frac{T_a}{\overline{T}_a}\right) \qquad \text{(S14) (Equation 8 in the manuscript)}$$

(S14) is the exponential advective travel time distribution with mean advective travel time $\overline{T}_a$.

Using (S14), the integral in (S13) evaluates to:

$$\int_0^\infty \exp\{-k(\omega)T_a\}P(T_a)dT_a = \frac{1}{1+k(\omega)\overline{T}_a} \qquad \text{(S15)}$$

To proceed further, I start from the denominator:

$$1+k(\omega)\overline{T}_a = 1+\left(i\omega+\frac{2\phi_m\sqrt{RD_e\omega}}{b}\sqrt{i}-\frac{\frac{4\phi_m\sqrt{RD_e\omega}}{b}\sqrt{i}}{\left(1+\exp\left(2\sqrt{\frac{R\omega}{D_e}}B\sqrt{i}\right)\right)}\right)\overline{T}_a \quad \text{(S16)}$$

To evaluate (S16), first note that

$$1+\exp\left(2\sqrt{\frac{R\omega}{D_e}}B\sqrt{i}\right) = 1+\exp\left(2\sqrt{\frac{R\omega}{D_e}}B\frac{1+i}{\sqrt{2}}\right) = 1+\exp\left(\sqrt{\frac{2R\omega}{D_e}}B\right)\left(\cos\left(\sqrt{\frac{2R\omega}{D_e}}B\right)+i\sin\left(\sqrt{\frac{2R\omega}{D_e}}B\right)\right)$$

Now, let

82 $$m = 1 + \exp\left(\sqrt{\frac{2R\omega}{D_e}}B\right)\cos\left(\sqrt{\frac{2R\omega}{D_e}}B\right), n = \exp\left(\sqrt{\frac{2R\omega}{D_e}}B\right)\sin\left(\sqrt{\frac{2R\omega}{D_e}}B\right)$$

83 Thus, $$1 + k(\omega)\overline{T}_a = 1 + \left(i\omega + \frac{2\phi_m\sqrt{RD_e\omega}}{b}\frac{1+i}{\sqrt{2}} - \frac{4\phi_m\sqrt{RD_e\omega}}{b}\frac{1+i}{\sqrt{2}}\frac{m-in}{m^2+n^2}\right)\overline{T}_a \qquad \text{(S17)}$$

84 The right side of (S17) can be rewritten after separating the real and imaginary parts, as:

85 $$\left(1 + \frac{\sqrt{2RD_e\omega}}{b}\phi_m\overline{T}_a\left(1 - \frac{2(m+n)}{m^2+n^2}\right)\right) + i\left(\omega\overline{T}_a + \frac{\sqrt{2RD_e\omega}}{b}\phi_m\overline{T}_a\left(1 - \frac{2(m-n)}{m^2+n^2}\right)\right)$$

86 Now, let $M = 1 - \frac{2(m+n)}{m^2+n^2}, N = 1 - \frac{2(m-n)}{m^2+n^2}, A = \frac{\phi_m\sqrt{RD_e\overline{T}_a}}{b}$.

87 We can thus write:

88 $$\frac{1}{1 + k(\omega)\overline{T}_a} = \frac{1}{\left(1 + \sqrt{2}AM\sqrt{\omega\overline{T}_a}\right) + i\left(\omega\overline{T}_a + \sqrt{2}AN\sqrt{\omega\overline{T}_a}\right)} \qquad \text{(S18)}$$

89 Finally, $S_{C_oC_o} / S_{C_iC_i}$ is obtained by evaluating the integral in Equation (14) of the manuscript,

$$\left|\int_0^\infty \exp\{-k(\omega)T_a\}P(T_a)\,dT_a\right|^2 = \left|\frac{1}{1 + k(\omega)\overline{T}_a}\right|^2 \qquad \text{(S19)}$$

90

$$= \frac{1}{1 + 2\sqrt{2}AM\sqrt{\omega\overline{T}_a} + 2A^2(M^2+N^2)\omega\overline{T}_a + 2\sqrt{2}AN\left(\omega\overline{T}_a\right)^{3/2} + \omega^2\overline{T}_a^{\,2}}$$

91

92 Equation (S19) leads to the power spectrum of stream concentration variations as Equation (15)

93 in the manuscript.

94 A simpler form of (S19) can be derived for the simpler special case of $B \to \infty$. For this case, the

95 boundary condition at $z = B$ in (S4) is replaced with the requirement that $\tilde{C}_m$ remains bounded.

96 This leads to a simpler expression for $\tilde{C}_m$:

$$\tilde{C}_m = \tilde{C}_f e^{-\sqrt{i}uz} \qquad \text{(S20)}$$

The simpler form of (S11) for this case is:

$$\frac{d\tilde{C}_f}{d\tau_a} + \left(i\omega + \frac{2\phi_m \sqrt{RD_e\omega}}{b}\sqrt{i} \right)\tilde{C}_f = 0 \qquad \text{(S21)}$$

The corresponding simpler form of (S17) is:

$$1 + k(\omega)\overline{T}_a = \left(1 + \frac{\sqrt{2RD_e\omega}}{b}\phi_m \overline{T}_a \right) + i\left(\omega\overline{T}_a + \frac{\sqrt{2RD_e\omega}}{b}\phi_m \overline{T}_a \right) \qquad \text{(S22)}$$

The spectral filter $S_{C_oC_o} / S_{C_iC_i}$ is then obtained as:

$$\left| \frac{1}{1 + k(\omega)\overline{T}_a} \right|^2 = \frac{1}{1 + 2\sqrt{2}A\sqrt{\omega\overline{T}_a} + 4A^2\omega\overline{T}_a + 2\sqrt{2}A\left(\omega\overline{T}_a\right)^{3/2} + \omega^2\overline{T}_a^{\,2}} \qquad \text{(S23)}$$

It is readily verified that (S19) reduces to (S23) when $B \to \infty$, in which case $M, N \to 1$.

In Dupuit flow systems with significant water table relief (i.e. significant increase in saturated thickness *H* from stream to divide), or in the case of deep-circulating groundwater flow, the exponential distribution is not a suitable model for the advective travel time distribution. A gamma distribution (especially with $\alpha < 1$), which has two parameters, provides a more flexible model of the advective travel time distribution in such cases. Equation (14) in the manuscript can be employed with any advective travel time distribution. Below, I present the spectral ratio $S_{C_oC_o} / S_{C_iC_i}$ for a gamma advective travel time distribution (rewritten in terms of the mean advective travel time $\overline{T}_a$):

$$P(T_a) = \frac{\alpha^\alpha}{\Gamma(\alpha)\overline{T}_a}\left(\frac{T_a}{\overline{T}_a} \right)^{\alpha-1} \exp\left(-\alpha\frac{T_a}{\overline{T}_a} \right) \qquad \text{(S24)}$$

114 Using (S24) in Equation (14) of the manuscript, the spectral ratio $S_{C_oC_o} / S_{C_iC_i}$ for a gamma

115 advective travel time distribution is obtained as:

$$\left|\int_0^\infty \exp\{-k(\omega)T_a\}P(T_a)\,dT_a\right|^2 = \left|\frac{\alpha^\alpha}{\left(\alpha + k(\omega)\overline{T}_a\right)^\alpha}\right|^2 =$$

116 $$\frac{\alpha^{2\alpha}}{\left(\alpha^2 + 2\sqrt{2}AM\alpha\sqrt{\omega\overline{T}_a} + 2A^2\left(M^2+N^2\right)\omega\overline{T}_a + 2\sqrt{2}AN\left(\omega\overline{T}_a\right)^{3/2} + \omega^2\overline{T}_a^2\right)^\alpha} \quad \text{(S25)}$$

117 Equation (S25) shows that matrix diffusion combined with a gamma distributed advective travel

118 times across streamlines leads to a richer variety of power-law exponents in stream concentration

119 spectra. For $\alpha = 1$, (S25) reduces to (S19). For strong matrix diffusion (A>>1), the third term in

120 the denominator dominates and the spectral ratio behaves as $1/\omega^\alpha$ for a large frequency range,

121 rather than $1/\omega$ as in (S19 or Equation 15 in the manuscript). For pure advection $(A \to 0)$, the

122 spectral filter reduces to $1/(1+\omega^2\beta^2)^\alpha$, where $\beta = \overline{T}_a / \alpha$; which is consistent with that of the

123 gamma distribution and behaves as $1/\omega^{2\alpha}$ at high frequencies. In general, when matrix diffusion

124 is strong, the spectral ratio behaves as $1/\omega^\alpha$, rather than the $1/\omega^{2\alpha}$ behavior of the

125 corresponding advective travel time distribution, i.e. the power-law exponent of the advective

126 travel time power spectrum is halved as a result of matrix diffusion.

127 **S.3 Review of the Laplace Transform Solutions to (S1) - (S4), relevant to the catchment**

128 **solute TTD *h(t)* (Equation 18 in the manuscript)**

129 Laplace transform solutions for transport with matrix diffusion in fractured rock date back to

130 Grisak and Pickens (1980), Tang et al. (1981) and Maloszewski and Zuber (1985). For

131 completeness, I present the specific forms of the Laplace transforms used in the manuscript here.

I use the following notation to denote a Laplace transform $\hat{f}(s)$ of a function $f(t)$ and the corresponding inverse transform, where t denotes time and s is the Laplace transform variable:

$$\mathcal{L}\{f(t)\}(s) = \hat{f}(s) = \int_0^\infty e^{-st} f(t)dt, \quad \mathcal{L}^{-1}\left\{\hat{f}(s)\right\}(t) = f(t)$$

The Laplace transform of the fracture concentration at the end of a streamline is defined as:

$$\mathcal{L}\left\{C_f(T_a, t; I_{T_a})\right\}(s) = \hat{C}_f(T_a, s; I_{T_a}) \quad \text{(S24)}$$

The corresponding inverse Laplace transform is defined by:

$$\mathcal{L}^{-1}\left\{\hat{C}_f(T_a, s; I_{T_a})\right\}(t) = C_f(T_a, t; I_{T_a}) \quad \text{(S25)}$$

For a Dirac Delta input function, i.e. $C_i(t) = \delta(t)$, solving (S1) - (S4) using Laplace transforms yields:

$$\hat{C}_f(T_a, s; I_{T_a}) = \exp\left(-\left(s + 2a\sqrt{s}\tanh\left(\sqrt{\frac{Rs}{D_e}}B\right)\right)T_a\right) \quad \text{(S26)}$$

where $a = \phi_m\sqrt{RD_e}/b$.

The corresponding inverse Laplace transform is:

$$C_f(T_a, t; I_{T_a}) = H(t - T_a)\,\mathcal{L}^{-1}\left\{\exp\left(-2a\sqrt{s}\tanh\left(\sqrt{\frac{Rs}{D_e}}B\right)T_a\right)\right\}(t - T_a) \quad \text{(S27)}$$

where $H(t - T_a)$ is the Heaviside function (0 for $t \le T_a$ and 1 for $t > T_a$). Thus, if the Green's function (solution for a Dirac delta input) for the coupled equations (S1-S4) is denoted as $H(t - T_a)g(T_a; t - T_a)$, the function $g(T_a; t - T_a)$ is defined as:

$$g(T_a; t - T_a) = \mathcal{L}^{-1}\left\{\exp\left(-2a\sqrt{s}\tanh\left(\sqrt{\frac{Rs}{D_e}}B\right)T_a\right)\right\}(t - T_a) \quad \text{(S28)}$$

For $B \to \infty$, the tanh term in (S28) becomes 1 and the inverse Laplace transform $\mathcal{L}^{-1}\left\{\exp\left(-2a\sqrt{s}T_a\right)\right\}\left(t-T_a\right)$ is obtained analytically (Maloszewski and Zuber, 1985) to yield:

$$g\left(T_a;t-T_a\right)=\frac{aT_a}{\sqrt{\pi}\left(t-T_a\right)^{3/2}}\exp\left(-\frac{a^2T_a^2}{\left(t-T_a\right)}\right) \quad \text{(S29) (Equation 17 in the manuscript)}$$

For finite *B*, the inverse Laplace transform can be written in an integral form (Maloszewski and Zuber, 1985), but is easier to evaluate by numerical inversion of (S28). I used a numerical inversion to evaluate $g\left(T_a;t-T_a\right)$ in (18) for cases with finite matrix width. The MATLAB function "talbot_inversion" (McClure, 2020) was used for numerical Laplace transform inversion. The implementation of the inversion algorithm was verified by computing $\mathcal{L}^{-1}\left\{\exp\left(-2a\sqrt{s}T_a\right)\right\}\left(t-T_a\right)$ numerically and verifying that it matches the analytical form (S29).

S.4. Non-dimensionalization and Approximate Analytical Forms for the solute TTD $h(t)$ with Exponential and Gamma Advective Travel Time Distributions $P(T_a)$ for infinite matrix widths ($B/\sqrt{De\overline{T}_a}$ >>1)

For infinite matrix widths, the general expression (18) for h(t) can be non-dimensionalized and written in terms of dimensionless total $\left(t^*=t/\overline{T_a}\right)$ and advective $\left(T_a^*=T_a/\overline{T_a}\right)$ travel times as:

$$h\left(t^*\right)\overline{T_a}=\int_0^{t^*}\frac{AT_a^*}{\sqrt{\pi}\left(t^*-T_a^*\right)^{3/2}}\exp\left(-\frac{A^2T_a^{*2}}{\left(t^*-T_a^*\right)}\right)\left(P\left(T_a^*\right)\overline{T_a}\right)dT_a^* \qquad \text{(S30)}$$

Note that $h\left(t^*\right)\overline{T_a}$ is the dimensionless solute TTD and $P\left(T_a^*\right)\overline{T_a}$ is the dimensionless advective travel time distribution. Also note that $A=\phi_m\sqrt{RD_e\overline{T}_a}/b=a\sqrt{\overline{T_a}}$, as defined in Equation (16) in the main manuscript. For exponential and gamma advective travel time distributions, the advective travel time distributions are rewritten in dimensionless form below:

Exponential: $$P\left(T_a^*\right)\overline{T_a} = \exp\left(-T_a^*\right) \quad \text{(S31)}$$

Gamma: $$P\left(T_a^*\right)\overline{T_a} = \frac{\alpha^\alpha}{\Gamma(\alpha)}\left(T_a^*\right)^{\alpha-1}\exp\left(-\alpha T_a^*\right) \quad \text{(S32)}$$

Numerical integration of (S30) was performed using the MATLAB function "integral" to obtain the exact dimensionless solute TTD.

There are three dimensionless time regimes in which simpler approximations to (S30) can be developed.

VERY EARLY TIME: As noted in the main manuscript, for very early times ($t^* << 1$), $h\left(t^*\right)\overline{T_a} \to P\left(t^*\right)\overline{T_a}$ for any form of the advective travel time distribution, because $g\left(T_a; t - T_a\right) \to \delta\left(t - T_a\right)$ at short times $(t, T_a \to 0)$. In other words, the solute TTD approaches the advective travel time distribution at very early times. The behavior is confirmed in Figure S1.

ANALYTICAL APPROXIMATION FOR $t^* > 1/A$: Approximate analytical forms of (S30) can be obtained after change of variables and asymptotic approximation of the resulting integral for $t^* > 1/A$ (Hyman et al. 2019):

Exponential: $$h\left(t^*\right)\overline{T_a} \approx \frac{1}{4A^2}\left(\frac{2A}{\sqrt{\pi t^*}} - \exp\left(\frac{t^*}{4A^2}\right)\operatorname{erfc}\left(\frac{\sqrt{t^*}}{2A}\right)\right) \quad \text{(S33)}$$

Gamma: $$h\left(t^*\right)\overline{T_a} \approx \left(\frac{\alpha}{2}\right)^{\alpha+1}\frac{\left(t^*\right)^{-1+\frac{\alpha}{2}}U\left(\frac{1+\alpha}{2}, \frac{1}{2}, \frac{\alpha^2 t^*}{4A^2}\right)}{A^\alpha\sqrt{\pi}} \quad \text{(S34)}$$

where $U(.,.,.)$ is the confluent hypergeometric function of the second kind (Weisstein, 2021), also known as the confluent hypergeometric Kummer U function. It should also be noted that (S33) is essentially a special case of (S34) for $\alpha = 1$, in as much as the exponential distribution is a special case of the gamma distribution for $\alpha = 1$.

Figure S1 shows comparisons between the exact $h\left(t^*\right)\overline{T_a}$ obtained by numerical integration of (S30) and analytical approximations (S33) and (S44). Figure S1 confirms that (S33) and (S34) are excellent approximations to the numerical integral of (S30) for $t^* > 1/A$.

The expressions (S33) and (S34) can be further approximated in intermediate and late time regimes.

INTERMEDIATE-TIME ($1/A < t^* < 4A^2/\alpha^2$) POWER LAW REGIME: An intermediate power-law regime prevails in the dimensionless time range $1/A < t^* < 4A^2/\alpha^2$ (note that this dimensionless time range may not exist for small values of A and larger values of α). This power-law regime is most clearly evident for $A = 10$ in Figure S1, but also for $A = 5$ and $\alpha = 1$, 0.7. From a MacLaurin series expansion of (S34), this power-law regime can be identified as

$$h\left(t^*\right)\overline{T_a} \approx \frac{\left(\alpha/2\right)^{\alpha+1}}{A^{\alpha}\Gamma\left(1+\frac{\alpha}{2}\right)}\left(t^*\right)^{-1+\frac{\alpha}{2}} \qquad \text{(S35)}$$

Equation (S35) is not plotted in Figure S1 to keep it from getting too crowded. Figure S2 shows a comparison between (S35) and (S30) for different values of α and A, and confirms its validity, especially for larger values of A and smaller values of α.

LATE-TIME ($t^* >> A^2$) BEHAVIOR AND POWER LAW REGIME: It is also evident from Figure S1 that at dimensionless times $t^* \sim A$, $h\left(t^*\right)\overline{T_a}$ becomes largely insensitive to the advective travel time distribution (i.e. α), and approaches a limiting distribution (controlled by matrix diffusion, with little dependence on the advective travel time distribution) for a given A. A late time power law regime is identified for $t^* >> A^2$, where further asymptotic expansion of

206 (S33) and (S44) produces the leading behavior shown in (S36) for any advective travel time
207 distribution, which is also verified in Figures S1 and S2.

208 $$h\left(t^*\right)\overline{T_a} \sim \frac{A}{\sqrt{\pi}t^{*3/2}} \qquad \text{(S36)}$$

209 However, this limit appears to be of limited practical value because it is only valid at very late
210 times when the influence of a finite matrix width may already be manifest.

211 IN SUMMARY: The general analytical approximations (S33) and (S34) are valid for $t^* > 1/A$,
212 and the approximate power law (S35) is valid for $1/A < t^* < 4A^2/\alpha^2$, when the values of A and
213 α are such that this time regime exists. For finite matrix widths, the influence of a finite matrix
214 is not experienced for $t^* < B^2/\left(D_e\overline{T}_a\right)$. Thus, the power law regime (S35) is valid even for
215 finite matrix widths, in the dimensionless time range $1/A < t^* < \min(B^2/\left(D_e\overline{T}_a\right), 4A^2/\alpha^2)$.
216 This behavior is evident in Figures 2b and 3b in the main manuscript, where the infinite and
217 finite matrix width cases follow the same solute TTD for a significant time range. At $t^* \sim A$,
218 $h\left(t^*\right)\overline{T_a}$ becomes largely insensitive to the advective travel time distribution (i.e. α), and
219 approaches a limiting distribution that only depends on A.

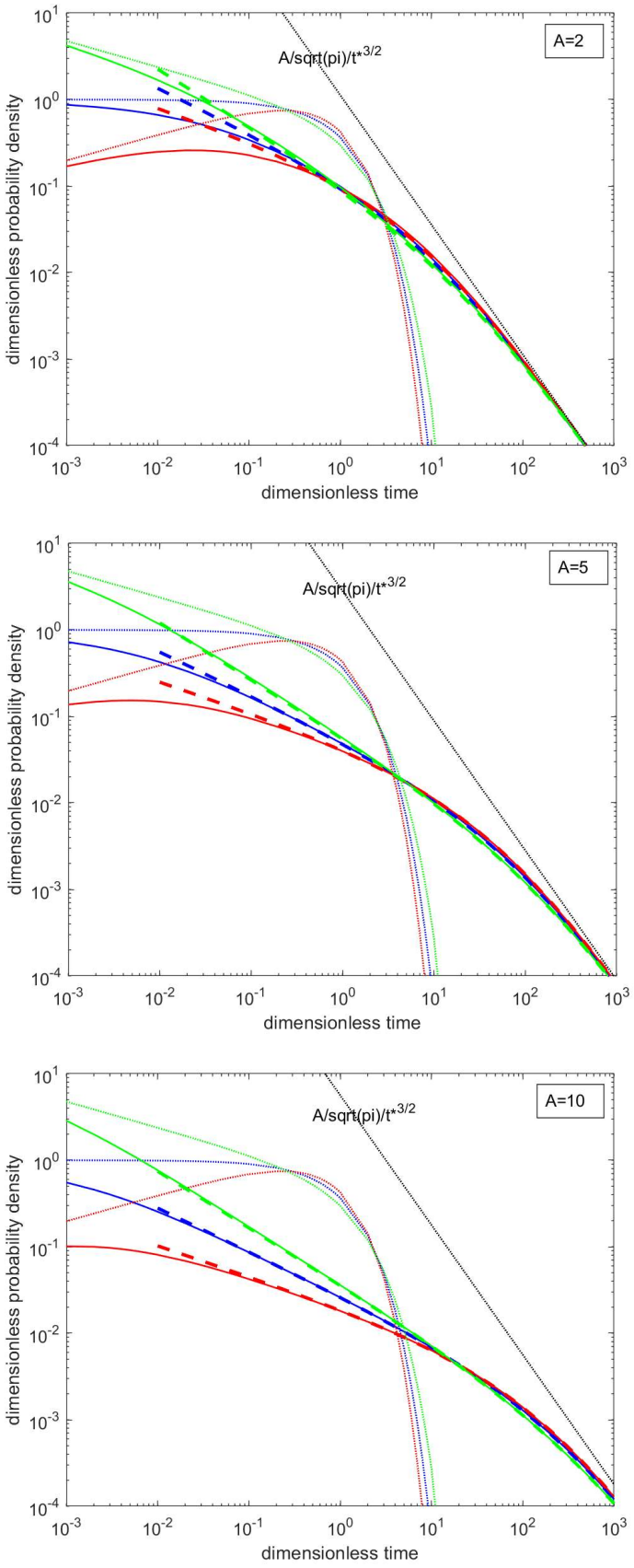

Figure S1. Dimensionless solute TTD $h\left(t^*\right)\overline{T_a}$ versus dimensionless time (t^*) for infinite matrix widths and different values of A, for gamma distributions with $\alpha = 0.7$ (green), 1 (blue) and 1.3 (red). Note that α =1 corresponds to the exponential distribution. Dotted lines: Dimensionless advective travel time distributions $P\left(T_a^*\right)\overline{T_a}$, Solid lines - Exact $h\left(t^*\right)\overline{T_a}$ from numerical integration of (S30), Dashed lines – Approximations (S33) and (S34). The straight line representing the late-time asymptote $h\left(t^*\right)\overline{T_a} \to A/\left(\sqrt{\pi}t^{*3/2}\right)$ (S36) is also shown.

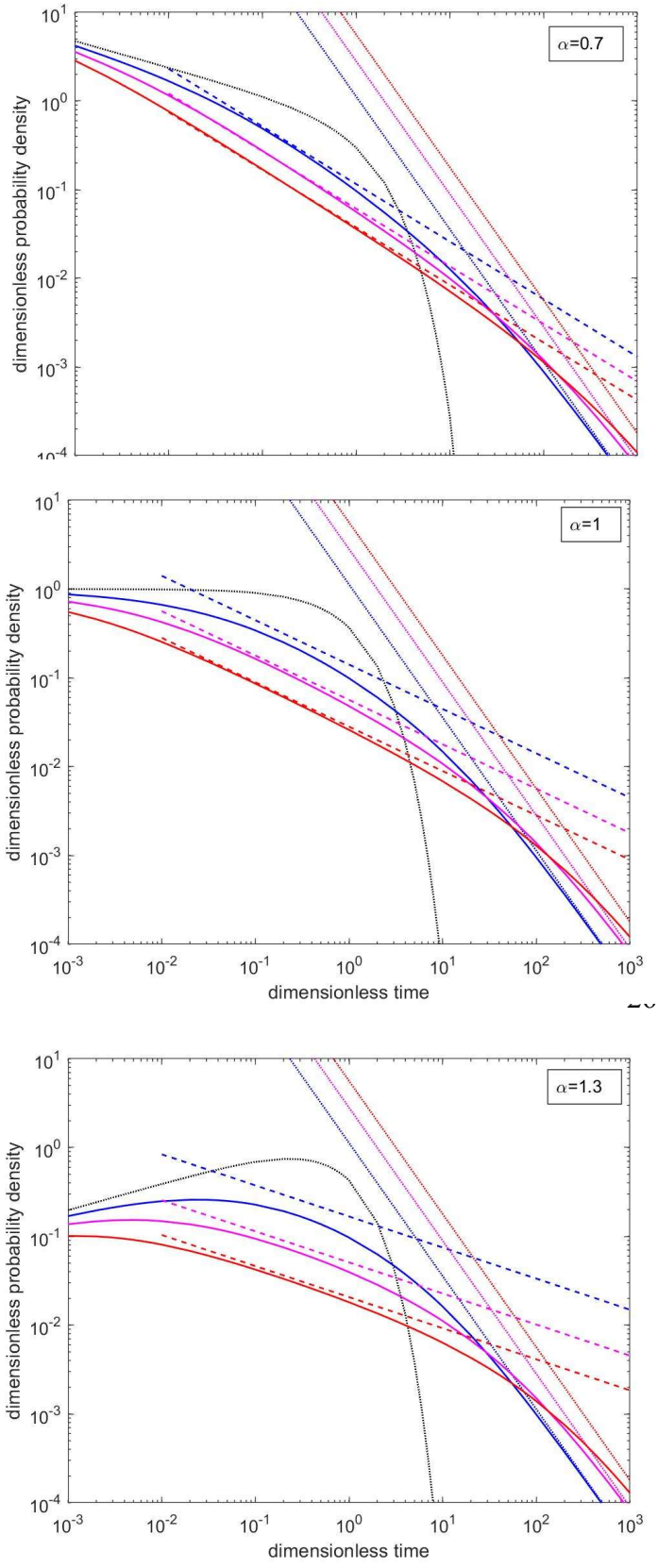

Figure S2. Dimensionless solute TTD $h\left(t^*\right)\overline{T_a}$ versus dimensionless time (t^*) for infinite matrix widths and gamma distributions with different values of α. For each value of α, the behavior is shown for different values of A, $A = 2$ (blue), 5 (magenta) and 10 (red). The dotted black line in each plot shows the advective travel time distributions $P\left(T_a^*\right)\overline{T_a}$ for the corresponding α.
Solid lines - Exact $h\left(t^*\right)\overline{T_a}$ from numerical integration of (S30),
Dashed lines – intermediate-time power-law approximation from (S35)
Dotted lines – very late time asymptote $h\left(t^*\right)\overline{T_a} \to A/\left(\sqrt{\pi}t^{*3/2}\right)$ (S36)

S.5 Stream Concentration Power Spectra Obtained with Alternative Parameter Sets for Lower Hafren

As noted in the main body of the paper, the power spectral ratio $S_{C_oC_o} / S_{C_iC_i}$ depends on two parameters, the mean advective travel time $\overline{T}_a$ and the matrix diffusion parameter A. The dimensionless parameter A involves products and ratios of other physical parameters. I present calculations of $S_{C_oC_o} / S_{C_iC_i}$ for two additional sets of parameters below. The rationale for these additional sets was simply that I used values of $\overline{T}_a$ = 0.5 and 2 times the value in the base case included in the main manuscript, and refitted other parameters to match the estimated stream concentration power spectrum in Figure (3a). The parameter values are shown in Table S.1.

	$\overline{T}_a$ (years)	ϕ_m	D_e (m^2/s)	b (m)	A
Base Case	0.01	0.15	1.5e-10	5e-4	2.06
Half $\overline{T}_a$	0.005	0.1	1.5e-10	2e-4	2.43
Double $\overline{T}_a$	0.02	0.05	1.5e-10	5e-4	0.97

Table S1. Alternative Parameter Combinations

Figure S3 shows the power spectra obtained with parameters in the second and third rows of Table S1. The "Half $\overline{T}_a$"parameter set produces an acceptable fit and improves the match to sample spectra at higher frequencies. The "Double $\overline{T}_a$" parameter set produces an acceptable fit with a larger mismatch compared to the base case at frequencies > 10^2 year^{-1}. The non-uniqueness involved in the estimating catchment-scale matrix diffusion parameters is acknowledged. However, the fitted parameter values are within acceptable ranges for these parameters. Figure S4 shows the power spectra obtained with the base case parameters and the alternative precipitation concentration power spectrum $0.38/f^{0.34}$ (mg/L)^2-yr.

(a)

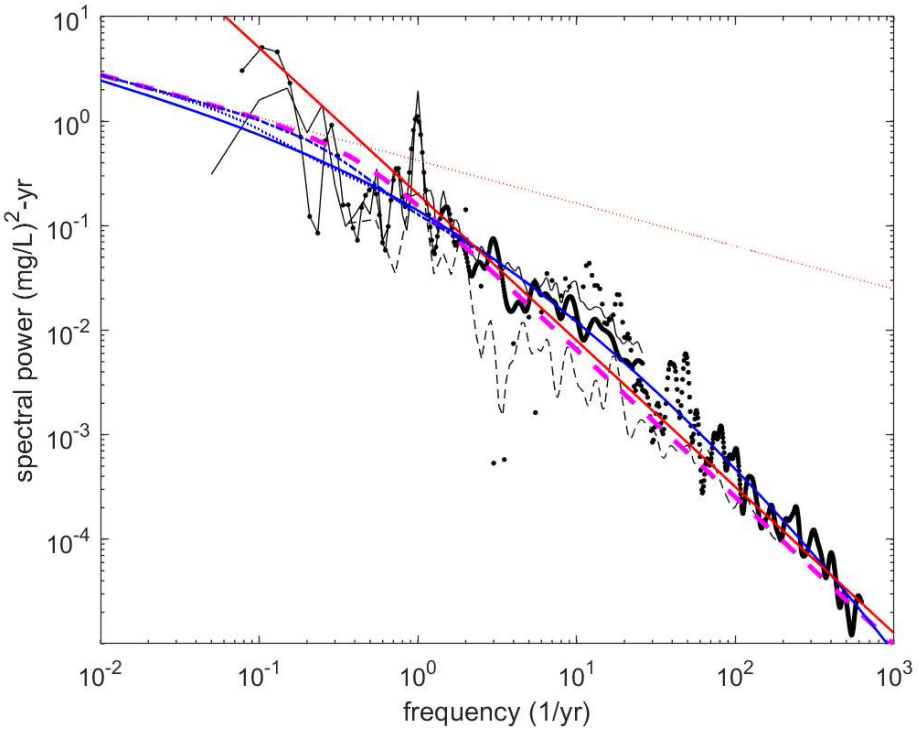

(b)

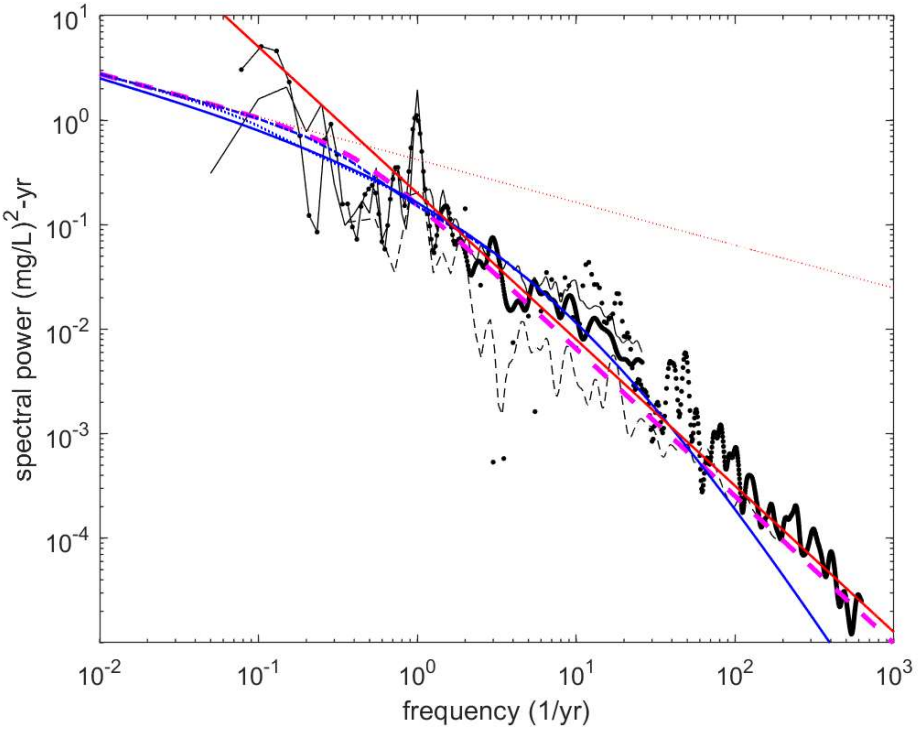

Figure S3. Stream (concentration power spectra calculated using alternative parameter sets shown in Table S1. (a) Half $\overline{T}_a$ and (b) Double $\overline{T}_a$, compared to $\overline{T}_a$ in the base case (Figure 3a in the main body of the paper). Color schemes are same as in Figure 3a. Black symbols and lines represent spectral estimates from Kirchner et al. (2013), magenta dashed line is the power spectrum corresponding to a gamma distribution ($\alpha = 0.5,\ \beta = 0.4\text{yr}$), blue lines are power spectra obtained from the matrix diffusion model (solid – infinite matrix, dashed – B = 0.1m,

dash-dotted – B = 0.05m), the red solid line indicates a spectral slope of -1.4, and the red dotted line shows the precipitation concentration spectrum.

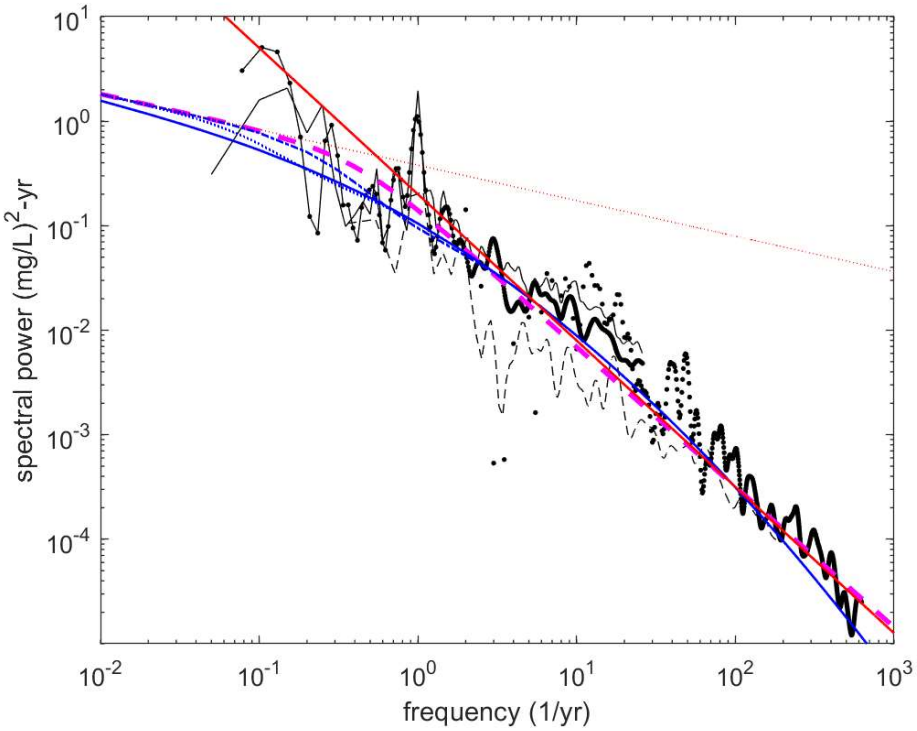

Figure S4. Stream concentration power spectra calculated using alternative precipitation chloride power spectrum $S_{C_iC_i}(f) = 0.38 / f^{0.34}$. Compared to Figure 3a, the differences are minor. Color schemes are same as in Figure 3a. Black symbols and lines represent spectral estimates from Kirchner et al. (2013), magenta dashed line is the power spectrum corresponding to a gamma distribution ($\alpha = 0.5$, $\beta = 0.4\,\mathrm{yr}$), blue lines are power spectra obtained from the matrix diffusion model (solid – infinite matrix, dashed – B = 0.1m, dash-dotted – B = 0.05m), the red solid line indicates a spectral slope of -1.4, and the red dotted line indicates the precipitation concentration spectrum.